

**RIGA TECHNICAL UNIVERSITY**

Faculty of Materials Science and Applied Chemistry

Institute of Inorganic Chemistry

Biomaterials Research Laboratory

**Agnese Brangule**

Doctoral Student of the Study Programme “Chemistry Technology”

**APPLICATION OF FOURIER TRANSFORM  
INFRARED SPECTROSCOPY IN ANALYSIS  
OF SYNTHESIZED AND NATURAL  
CALCIUM PHOSPHATE**

**Summary of the Doctoral Thesis**

Scientific supervisor:

Assoc. Professor, *Dr. sc. ing.*

**KĀRLIS AGRIS GROSS**

**RTU Press  
Riga 2017**

Brangule A. Application of Fourier Transform Infrared Spectroscopy in Analysis of Synthesised and Natural Calcium Phosphate. – Riga: RTU Press, 2017 – 54 p.

Published in accordance with the Decision of the Promotion Council “RTU P-02” of 4 October 2017,  
Minutes No 04030-9.2.1/4.

**ISBN 978-9934-22-028-9**

**DOCTORAL THESIS  
PROPOSED TO RIGA TECHNICAL UNIVERSITY  
FOR THE PROMOTION TO THE SCIENTIFIC DEGREE OF  
DOCTOR OF ENGINEERING SCIENCES**

To be granted the scientific degree of Doctor of Engineering Sciences, the present Doctoral Thesis has been submitted for the defence at the open meeting of RTU Promotion Council on \_\_\_\_\_ 2017 at the Faculty of Materials Science and Applied Chemistry of Riga Technical University, 3 Paula Valdena Street, Room 272.

**OFFICIAL REVIEWERS**

Professor, Dr. habil. sc. ing. Gundars Mežinskis  
Institute of Silicate Materials, Riga Technical University

Professor, Dr. habil. Sigitas Tamulevičius  
Institute of Materials Science, Kaunas University of Technology, Lithuania

Professor, Dr. habil. chem. Andris Zicmanis  
Faculty of Organisc Chemistry, University of Latvia

**DECLARATION OF ACADEMIC INTEGRITY**

I hereby declare that the Doctoral Thesis submitted for the review to Riga Technical University for the promotion to the scientific degree of Doctor of Engineering Sciences is my own. I confirm that this Doctoral Thesis had not been submitted to any other university for the promotion to a scientific degree.

Agnese Brangule .....

Date: .....

The Doctoral Thesis has been written in Latvian. It consists of Introduction, 3 Chapters: Literature review (six subchapters), Experimental part (three subchapters), Results and Discussion (four subchapters), Conclusions and References. The total number of pages is 147 pages. The Bibliography contains 195 titles.

## ACKNOWLEDGEMENT

I express my gratitude to my scientific supervisor **Assoc. Professor, Dr. sc. ing. Kārlis Agris Gross** for an opportunity to carry out research in the field of calcium phosphates and biomaterials.

I would like to thank everyone who shared knowledge, inspired, supported and helped me throughout all these years.

**Prof. Arturs Vīksna** from the Department of Analytical Chemistry of the University of Latvia (Riga, Latvia), **Prof. Andris Actiņš** and **Dr. chem. Agris Bērziņš** from the Department of Physical Chemistry of the University of Latvia, **Prof. Aivaras Kareiva** and his group from the Department of Inorganic Chemistry of the University of Vilnius.

I express my gratitude to the employees of the Department of Biology and Microbiology of Rīga Stradiņš University **Dr. med. Ingus Skadiņš** and **Dr. med. Aigars Reinis** for collaboration in assessment of bacterial interactions with the material developed.

I express my gratitude to **Dr. hist. Gunita Zariņa**, Institute of History of Latvia, and **Prof. Māra Pilmane**, Director of the Institute of Anatomy and Anthropology (IAA) and Head of the Department of Morphology, for an opportunity to access contemporary and archaeological bone materials.

I express my gratitude to **Prof. Pēteris Tretjakovs**, Head of the Department of Human Physiology and Biochemistry of Riga Stradins University for the support in conference visits and motivating to lead the doctorate thoroughly.

I express my gratitude to the personnel of the Rūdolfs Cimdiņš Riga Biomaterials Innovation and Development Centre of RTU and **Dr. sc. ing. Jānis Ločs** for supporting the development of the Doctoral Thesis.

I express my gratitude to **Dr. chem. Gunta Ķizāne**, Head of the Department of Radiation Processes of the Institute of Chemical Physics of the University of Latvia, and researchers **Artūrs Zariņš**, **Līga Avotiņa** and **Mihails Halitovs** for their interest and support to all my ideas.

I express my gratitude to **Assoc. Professor, Dr. chem. Daina Kalniņa**, RTU, for the long discussions in the field of calcium phosphates.

I would like to express my heartfelt thanks to my family, who did everything possible to support and motivate me to develop and complete the work.

# CONTENTS

ACKNOWLEDGEMENT .....	4
Abbreviations and definitions .....	6
GENERAL CHARACTERISTICS OF THE WORK .....	7
Introduction .....	7
Aim of the Doctoral Thesis .....	7
Tasks of the Doctoral Thesis .....	7
Theses to be Defended .....	8
Scientific Novelty .....	8
Practical Significance .....	8
Approbation of the Results .....	9
List of Publications .....	9
Presentations at International Conferences with Published Abstracts .....	9
LITERATURE REVIEW .....	11
EXPERIMENTAL PART .....	15
RESULTS AND DISCUSSION .....	17
1. Development and Assessment of the Comparison Model of FTIR Methods for Nanosized Calcium Phosphate Research. ....	17
1.1. Development of the Model for the Mutual Qualitative and Quantitative Comparison of Different FTIR Methods .....	17
1.2. Qualitative Analysis of FTIR Spectra .....	18
1.3. Quantitative (statistical) Analysis of the FTIR Spectra .....	19
1.4. Model Assessment and Usage Options .....	24
2. Thermokinetic Studies of Nanosized Calcium Phosphate .....	27
2.1. Optimization of Drying Process Control .....	28
2.2. Changes in Content of Carbonate Ions Due to Temperature .....	33
3. Development and Approbation of the Deconvolution Model .....	38
3.1. Development of the Deconvolution Model .....	38
3.2. Assessment of the Deconvolution Model .....	40
4. Advantages of Using PAS and DRIFT Spectroscopy in the Study of Nanosized Calcium Phosphates .....	43
4.1. Characterization of Microsamples .....	43
4.2. Processes in Volume .....	44
4.3. Characterization of Wet and Contaminated Samples .....	46
4.4. Processes on the Surface of Calcium Phosphates .....	46
CONCLUSION .....	49
REFERENCES .....	50
APPENDIX .....	52

## ABBREVIATIONS AND DEFINITIONS

ACP – amorphous calcium phosphate  
AHCA – agglomerative hierarchical cluster analysis  
CACP – amorphous calcium phosphate containing carbonate ions  
CaP – calcium phosphates  
CCP – calcium phosphate containing carbonate ions  
CI – crystallinity index  
DHCA – distributed hierarchical cluster analysis  
DoE – design of experiments  
DSC – differential scanning calorimetry  
DTA – differential thermal analysis  
FSD –Fourier self-deconvolution  
FTIR –Fourier Transform Infrared Spectroscopy  
FTIR ATR – Fourier Transform Infrared Attenuated Total Reflection Spectroscopy  
FTIR DRIFT – Diffuse Reflectance Infrared Fourier Transform Spectroscopy  
FTIR KBr – Fourier Transform Infrared Transmission Spectroscopy, pressed in a KBr tablet  
FTIR PAS – Fourier Transform Infrared Photoacoustic spectroscopy  
HAp – hydroxyapatite  
HCA – hierarchical cluster analysis  
HPLC – high performance liquid chromatography  
ICP – inductively coupled plasma spectrometry  
IS – infrared radiation  
KM – Kubelka-Munk units  
MS – mass spectrometry  
PAT – process analytical technology  
PC – principal component  
PCA – principal component analysis  
PKK – Pearson correlation coefficient  
QbD – quality by design  
SEM – scanning electron microscopy  
SF – separation factor  
TCP – tricalcium phosphate  
TG – thermogravimetry  
TTCP – tetracalcium phosphate  
TXRF – total reflection X-ray fluorescence  
XRD – powder X-ray diffractometry

# GENERAL CHARACTERISTICS OF THE WORK

## Introduction

Extensive research on hydroxyapatite and other calcium phosphates in the field of biomaterials has been taking place for over 50 years. However, only in the last 10 years there has been wider understanding of the influence of the structure of apatites on the biocompatibility of the material. Therefore, great attention is paid to the modification of existing materials, the creation of new materials and comprehensive characterization.

Insufficient attention is still being paid to the convenient and efficient characterization of the structure and quality of nanosized calcium phosphates. With the development of spectroscopic analytical methods and IT technologies, it is possible to obtain more accurate data on synthesized material. For instance, Fourier Transform Infrared Spectroscopy (FTIR) techniques, which can provide not only qualitative, but also quantitative information about a sample in a very short time, combined with statistical methods, provide a convenient graphical and visual representation of the data. Although over the past 20 years the usage of statistical methods in the analysis of spectroscopic data has increased more than 10 times (number of article on the usage of statistical methods in FTIR spectroscopy indexed in SCOPUS database in 1996 was 20, but in 2016 it was 232), however, it has been unreasonably forgotten in studies of calcium phosphates. Possibly the lack of the quality of the spectra does not allow to use it.

The results of the doctoral dissertation substantiate the high potential of data multi-factorial analysis in both calcium phosphate production and research process, as it allows more detailed analysis of the obtained data and prediction of physico-chemical properties of the material.

In this work, an innovative FTIR cantilever-enhanced photoacoustic spectroscopy (PAS) method has been used, which was first used in spectroscopic studies of both calcium phosphates and bacteria. Cantilever-enhanced photoacoustic detectors developed and patented by GASERA Ltd. are used to develop completely new analytical methods in a number of innovative EU-funded projects (such as IRON, HORIZON 2020 EU-PROJECT, and DOGGIE and CUSTUM).

## Aim of the Doctoral Thesis

To develop the control methods of the process of nanostructured hydroxyapatite synthesis using innovative FTIR spectrometry and statistical data processing methods, providing high payout efficiency and wide application capability.

## Tasks of the Doctoral Thesis

1. To carry out systematic studies on the application of FTIR spectroscopic and multi-factor data analysis for nanostructured calcium phosphates.
2. To evaluate the effect of drying conditions on the structure of calcium phosphate compared to the results obtained by the FTIR with the results of XRD and TG and give recommendations on optimal drying conditions for the synthesis of amorphous or microcrystalline substances.
3. To evaluate the benefits of using the FTIR spectroscopy method, the purity of calcium phosphate, the degree of crystallinity and structures (e.g.,  $\text{PO}_4^{3-}$ , A, B-type  $\text{CO}_3^{2-}$ -A, B-type) for simultaneous control.

4. To evaluate the potential of using the FTIR PAS method for kinetic control of the chemical or physical process, for control of calcium phosphate contamination, for studies of surface and microsamples and biological activity.

## **Theses to be Defended**

The FTIR method is an effective method for controlling the result of the synthesis of nanosized calcium phosphates, which provides comprehensive characterization of the material, providing new research and process control capabilities.

FTIR spectroscopic methods together with methods of statistical data analysis provide high-performance data processing and automation capabilities.

FTIR PAS provides new non-destructive possibilities for surface studies of pressed/moulded or 3D-printed nano-sized calcium phosphate, which are not possible with previously used FTIR sampling techniques (ATR, DRIFT, KBr).

## **Scientific Novelty**

The developed FTIR spectroscopic data processing model provides efficient data processing, replacing other physico-chemical methods for determining key quality parameters and providing more information at a shorter analysis time.

For the first time, the FTIR PAS method has been developed, which allows simultaneous investigation of both the surface of calcium phosphate and microbiological samples on it.

For the first time, systematic and complex studies and evaluations of the relationships between the nanosized calcium phosphate spectra of different degrees of crystallinity obtained by different FTIR methods were conducted including the innovative cantilever-enhanced FTIR PAS in the studies.

For the first time, based on the FTIR and XRD spectra of calcium phosphates of varying degrees of crystallinity, the statistical model of the main components (PCA) was developed, which allows us to evaluate the degree of crystallinity and particle size of unknown CaP.

For the first time, an optimized method for determining the degree of crystallinity (index) of calcium phosphates is proposed, complementing the existing method with the peak deconvolution of the FTIR spectrum.

## **Practical Significance**

The research results provide an opportunity to comprehensively and with payout efficiency control the process of amorphous and microcrystalline HAP synthesis, control the conformity of the result of synthesis with the set objectives, determining the degree of crystallinity of the material obtained at the same time, contamination with the raw materials of the synthesis and drying process, avoiding time-consuming analytical steps or expensive additional equipment. The proposed methodology reduces the cost of control and provides extensive information on the qualitative parameters of nano-sized calcium phosphates. The results of the work prove the new possibilities of PAS FTIR providing more research opportunities.

## Approbation of the Results

The scientific achievements and main results of the doctoral thesis have been reflected in 7 full-text scientific publications and reported at 17 international scientific conferences (18 reviewed scientific conference theses).

## List of Publications

1. Brangule, A., Skadiņš, I., Reinis, A., Kroiča, J., Gross, K., *In vitro* characterization perspectives using Fourier transform infrared photoacoustic spectroscopy (FTIR PAS), *Key Engineering Materials*, **2017**, Vol. 758, pp. 273–277. Doi:10.4028/www.scientific.net/KEM.758.273, (**Scopus**).
2. Brangule, A., Avotiņa, A., Zariņš, A., Haļitovs, M., Gross, K., Ķizāne, G. Thermokinetic investigation of the drying conditions on amorphous calcium phosphate, *Key Engineering Materials*, **2017**, Vol. 758, pp. 204–209. Doi:10.4028/www.scientific.net/KEM.758.204, (**Scopus**).
3. Brangule, A., Gross, K., Stepanova V. Cantilever-enhanced photoacoustic spectroscopy applied in the research of natural and synthetic calcium phosphate. *IOP Conf. Ser.: Journal of Physics.*, **2017**, Vol. 829, (**Scopus**).
4. Brangule, A., Gross, K., Skadiņš, I., Reinis, A., Kroiča, J. Simultaneous Identification of Amorphous Calcium Phosphate and S.epidermidis Bacteria by Photoacoustic Spectroscopy. *Key Engineering Materials*, **2016**, Vol. 720, pp. 125–129. Doi:10.4028/www.scientific.net/KEM.720.125, (**Scopus**).
5. Brangule, A., Gross, K., Importance of FTIR spectra deconvolution for the analysis of amorphous calcium phosphates. *IOP Conf. Ser.: Materials Science and Engineering*, **2015**, 77(1). Doi:10.1088/1757-899X/77/1/012027, (**Scopus**).
6. Brangule, A., Gross, K., Effect on drying conditions on amorphous calcium phosphate. *Key Engineering Materials*, **2015**, Vol. 631, pp. 99–103. Doi:10.4028/www.scientific.net/KEM.631.99, (**Scopus**).
7. Brangule, A., Gross, K., Komarovska, L., Viksna, A. Exploring zinc apatites through different synthesis routes. *Key Engineering Materials*, **2014**, 587, pp. 171–176. Doi:10.4028/www.scientific.net/KEM.587.171, (**Scopus**).

## Presentations at International Conferences with Published Abstracts

1. Brangule, A., Avotiņa, A., Zariņš, A., Haļitovs, M., Gross, K., Ķizāne, G. Thermokinetic investigation of the drying conditions on amorphous calcium phosphate, *29<sup>th</sup> Symposium and Annual Meeting of the International Society for Ceramics in Medicine (BIOCERAMICS 29)*. France, Tuluza, 25–27 October, **2017**.
2. Brangule, A., Skadiņš, I., Reinis, A., Kroiča, J., Gross, K., *In vitro* characterization perspectives using Fourier transform infrared photoacoustic spectroscopy (FTIR PAS), *29<sup>th</sup> Symposium and Annual Meeting of the International Society for Ceramics in Medicine (BIOCERAMICS 29)*. France, Tuluza, 25–27 October, **2017**.
3. Brangule, A., Gross, K. Application of FTIR spectroscopy to the control of nanosized calcium phosphate synthesis, International Conference Nanotechnology and Innovation in the Baltic Sea Region, Lithuania, Kaunas, 14–16 June, **2017**.

4. Brangule, A., Gross, K. FTIR spektru apstrādes metodes un hemometrijas izmantošana kalcija fosfātu pētniecībā, 75<sup>th</sup> Annual Conference of the University of Latvia, 9 February, Latvia, Rīga, **2017**.
5. Brangule, A., Gross, K., Stepanova, V. Cantilever-enhanced photoacoustic spectroscopy applied in the research of natural and synthetic calcium phosphate Applied Nanotechnology and Nanoscience International Conference (ANNIC 2016), Spain, Barcelona, 9–11 November, **2016**.
6. Brangule, A., Gross, K., How Statistical Methods Guide the Selection of FTIR Methods Chemistry and Chemical Technology 2016, International conference of Lithuanian Society of Chemistry, Lithuania, Vilnius, 28–29 April, **2016**.
7. Brangule, A., Gross, K., Ūbele, D. A Measure of Crystallinity in Nanosized Calcium Phosphate, *Riga Technical University 57<sup>th</sup> International Scientific Conference*, Latvia, Riga, 21 October, **2016**.
8. Brangule, A., Gross, K., Skadiņš I., Reinis, A., Kroiča, J. Simultaneous Identification of Amorphous Calcium Phosphate and *S.epidermidis* Bacteria by Photoacoustic Spectroscopy, *28<sup>th</sup> Symposium and Annual Meeting of the International Society for Ceramics in Medicine (BIOCERAMICS 28)*. USA, North Caroline, Charlotte, 18–21 October, **2016**.
9. Brangule, A., Gross, K., Spectroscopic characterization of natural calcium phosphates by FTIR-DRIFT, *8th Annual meeting of the Scandinavian Society for Biomaterials*, Latvia, Sigulda, 6–8 May, **2015**.
10. Brangule, A., Gross, K., Characterization of Calcium Phosphates with Photoacoustic Spectroscopy, *Riga Technical University 56<sup>th</sup> International Scientific Conference*, Latvia, Riga, 14–17 October, **2015**.
11. Brangule, A., Zariņa, G. Importance of FTIR Spectra Deconvolution in Characterization of Bones and Synthesized Bone Materials. *3<sup>rd</sup> Baltic Bioarchaeology Meeting*. Latvia, Riga, 15–16 April, **2014**.
12. Brangule, A., Gross, K., Effect on drying conditions on amorphous calcium phosphate. *26<sup>th</sup> Symposium and Annual Meeting of the International Society for Ceramics in Medicine (BIOCERAMICS 26)*, Spain, Barcelona, 6–8 November, **2014**.
13. Brangule, A., Gross, K., Importance of FTIR Spectra Deconvolution in Amorphous Calcium Phosphate Analysis, *Joint International Symposium RCBJSF – 2014 - FM&NT*, Latvia, Riga, 29 September – 2 October, **2014**.
14. Brangule, A., Gross, K., Advantages of FTIR-DRIFT sampling in calcium phosphate research, *Ecobalt 2014*, Latvia, Riga, 8–10 October, **2014**.
15. Brangule, A., Gross, K., Ūbele, D., Comparison of FTIR methods for analyzing calcium phosphates, *Riga Technical University 55<sup>th</sup> International Scientific Conference*, Latvia, Riga, 14–17 October, **2014**.
16. Gross, K.A., Brangule, A., Komarovska, L., Viksna, A. Exploring zinc incorporation in apatite for orthopedics and dentistry (*Standing report*). *18th International scientific conference EcoBalt 2013*, Lithuania, Vilnius, 25–27 October, **2013**.
17. Brangule, A., Gross, K., Komarovska, L., Viksna, A. Exploring zinc apatites through different synthesis routes. *25<sup>th</sup> Symposium and Annual Meeting of the International Society for Ceramics in Medicine (BIOCERAMICS 25)*, Romania, Bucharest, 7–10 November, **2013**.

## LITERATURE REVIEW

**Modern production process.** With the development of technology and communication, not only the technological process and capabilities change, but also the communication between the producer and the consumer is changing. A modern production process determines that:

1. the manufacturer (the offer) must anticipate the consumer's (demand) needs;
2. the quality is a key parameter that determines market success and creates communication between the supplier and the consumer [1].

The production process of the 21st century is based on an evidence-based quality control not only at the very end of the process, it is integrated into products by designing the quality in the production process – Quality by Design (QbD). The process analytical technology (PAT) is a technology that ensures the “translation” of the designed quality (QbD) in the real production process [2].

The PAT technology is not limited to the use of one device only [3]. This technology covers a variety of “tools” such as, multidimensional statistical analysis for data collection, processing and visualization, product quality assessment, continuous improvement of the production process and knowledge management (Fig. 1).

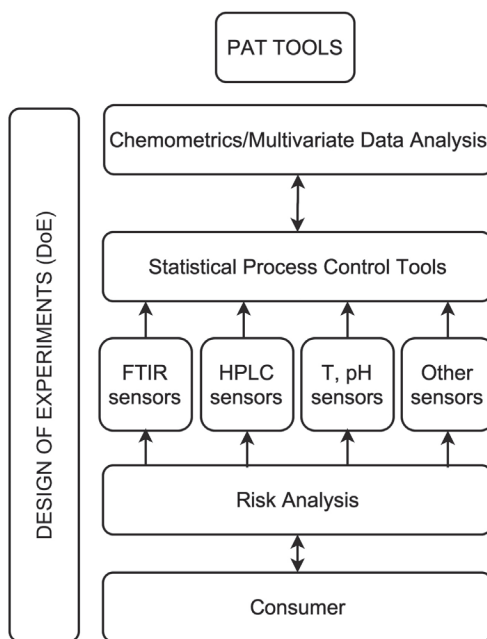


Fig. 1 The PAT toolbox [3]

The essential “tools” for online research (on-line) are:

- a) spectroscopic methods or sensors for characterization of the material or substance;
- b) smart sensors that measure production parameters.

The information provided by these sensors is used to create mathematical models. This is proof that the quality of the production process is determined not only by modern equipment but also by mathematical models and algorithms [4]. However, in order for such

a system to be managed not only by narrow-sector specialists but also by manufacturers, the analytical control (PAT) of the process must meet the following requirements: user-friendliness; unified documentation and traceability; no non-proprietary solution; standardized interface; neglectable matrix effects and interferences; appropriate accuracy; customized asset management functions; compliance with security (explosion proof, safe) requirements; robustness and industrial applicability; low maintenance costs; availability and long-term stability[5].

### **The use of Fourier Transform Infrared (FTIR) spectroscopy.**

Different methods, such as FTIR, XRD, Raman, etc. were used for the study and characterization of calcium phosphates. FTIR is a method that has been widely used in calcium phosphates research since the sixties of the 20th century [6], [7] and can be used for both qualitative and quantitative analysis [8].

The most commonly mentioned advantages of the FTIR method directly for calcium phosphates research are the following: the method is sensitive and non-destructive or only slightly damages the sample; it does not require sample preparation or it is minimal; small sample quantities are necessary for measuring [9]. Several FTIR sampling methods were evaluated in this work, with the highest emphasis on the usage of FTIR PAS and FTIR DRIFT. The advantages of both methods are the following: no sample preparation is needed; there is no contamination of the sample; there are small sample quantities; high sensitivity and the surface can also be measured with the PAS method.

**Photoacoustic Spectroscopy (PAS).** Photoacoustic spectroscopy is based on the photoacoustic effect, which was discovered in 1880 by scientist A. G. Bell. If the substance is irradiated with a pulsating light, the substance emits acoustic waves that have the same frequency as the pulsating light. In subsequent experiments, he added a hearing tube and fixed sounds [10]. A. G. Bell's initial works encouraged such scientists and researchers as Roentgen, Tyndall and Price to do the research in the field of photoacoustic spectroscopy.

In this work, the innovative cantilever – enhanced PAS was used. In 2003, the silicon console, invented by J. Kaupinen's group, replaced the less sensitive microphone membrane. In addition, the movement of the console could be read with both the optical beam deviation and the interferometer. The J. Kaupinen's group chose the interferometric reading because it offered a larger dynamic range (Fig. 2) [11].

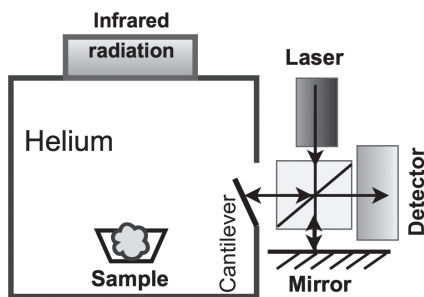


Fig. 2. The principal scheme of PAS with the cantilever-enhanced detector.

**Calcium phosphate biomaterials.** It is possible to design and synthesize bone or tissue-like materials by imitating nature. These smart materials can be used to develop innovative third-generation biomaterials [12]. Biomaterials or biocompatible materials are mainly biomimetic materials that can not only interact with biomaterials (for example, tissues, bones) but also imitate or even improve their functions [13]. The structure of mammalian bones and teeth is often compared to the structure of apatites, as evidenced by the use of diffractograms of mineral hydroxyapatite and by analyzing the ratio of calcium and phosphorus in apatite [14]. The stoichiometric calcium hydroxyapatite (HAp),  $\text{Ca}_{10}(\text{PO}_4)_6(\text{OH})_2$  is considered as an idealized bone and dental inorganic composition model [7]. Studies have emphasized that natural and synthetic apatites, however, differ substantially from the idealized HAp model not only by structure, composition, degree of ordering and particle size, but also by physical and chemical properties [15]. Therefore, in this work, as an inorganic bone composition model, amorphous calcium phosphate (ACP) and ACP and HAp compounds containing carbonate ions, which by composition and properties are more intrinsic to the inorganic part of the bone than pure hydroxyapatite, are mainly considered.

During the synthesis and production of calcium phosphates, drying is an integral part of the production process as synthesis, since drying affects the size, crystallinity, composition, structure and phase purity of the filtered particles. The most commonly used drying conditions are lyophilization ( $-50\text{ }^\circ\text{C}$ , vacuum, 48–72 h) [16], and air drying at various temperatures such as room temperature [17],  $70\text{--}90\text{ }^\circ\text{C}$ , 15–24 h [18],  $100\text{--}150\text{ }^\circ\text{C}$ , 24–48 h [19] or rinsing of precipitates with an organic solvent: alcohol or acetone, followed by drying at  $> 100\text{ }^\circ\text{C}$  [20]. The drying process also significantly affects the composition of the physically and chemically bound water in calcium phosphate. Therefore, in this work, the effect of the drying process on the amorphous and microcrystalline structure using not only FTIR methods but also DTG and MS are studied.

**Spectrum processing and multidimensional statistical analysis.** FTIR spectroscopy, in conjunction with multidimensional analysis, offers a very wide scope for both calcium phosphate and *in vitro* studies. Nowadays, data processing is usually carried out using computer based technologies and ready-made software. The main tasks of the author are: 1) to select the method most suitable for the research and the corresponding program or programs; and 2) to evaluate, correctly explain and interpret the results. The FTIR spectrum processing is essential, which can be divided into two stages:

- **pre-processing of the spectra** (background correction, spectrum alignment, normalization) needed to improve the appearance of spectra and increase spectrum interpretation and analysis;
- **spectrum processing** (derivation, deconvolution, and Fourier self-deconvolution) required to mathematically improve resolution when equipment options are already exhausted [21].

The main tasks of the multidimensional analysis are the following:

- 1) description of data and modeling of the structure of general data matrix;
- 2) discrimination, classification and grouping of data to divide all data into two or more groups (objects);
- 3) regression and forecasting; a method that binds two variables by quantifying them with each other [22].

FTIR spectra can be represented in the form of a data matrix, where the columns represent wavelengths (variables), but the rows represent observations (spectra). This means that each spectrum can be represented as a row of numbers in the matrix [23]. This work examines the unsupervised method of multidimensional analysis. Its task is to look for correlations in large data sets and in unmatched data matrices without the need for standard samples [24]. The unsupervised data processing method can be used for model creation and as a pre-processing for supervised data analysis [22]. Unsupervised methods are, for instance, the analysis of key components in PCA, hierarchical cluster analysis, HCA and Pearson correlation coefficient analysis in PKK [25].

## EXPERIMENTAL PART

The scheme of the doctoral thesis is shown in Fig 3.

The main research method in this work is the Fourier Transform Infrared Spectroscopy. Four FTIR sampling methods were used to study the synthesized and natural calcium phosphates: console type PAS, DRIFT, ATR and FTIR-KBr. The experimental part deals with evaluation and validation of the resolution of FTIR methods. A precision and repeatability test was performed.

Other research methods used in the work are:

- X-ray diffractometry (XRD) to judge the qualitative and quantitative composition of phases, product crystallinity and particle size; the Profex3.10.2 program for Rietveld analysis was used;
- thermogravimetry (TG/DTA) for the determination of chemically and physically bound water and for the determination of the composition and purity of the substance;
- scanning electron microscopy (SEM) for the surface analysis of pressed calcium phosphate, the analysis of the microbiological sample and the evaluation of Ca/P quantitative composition;
- mass spectroscopy for determination of purity of synthesized and dried under different conditions calcium phosphate, analysis of thermal stability and determination of molar mass of impurities.

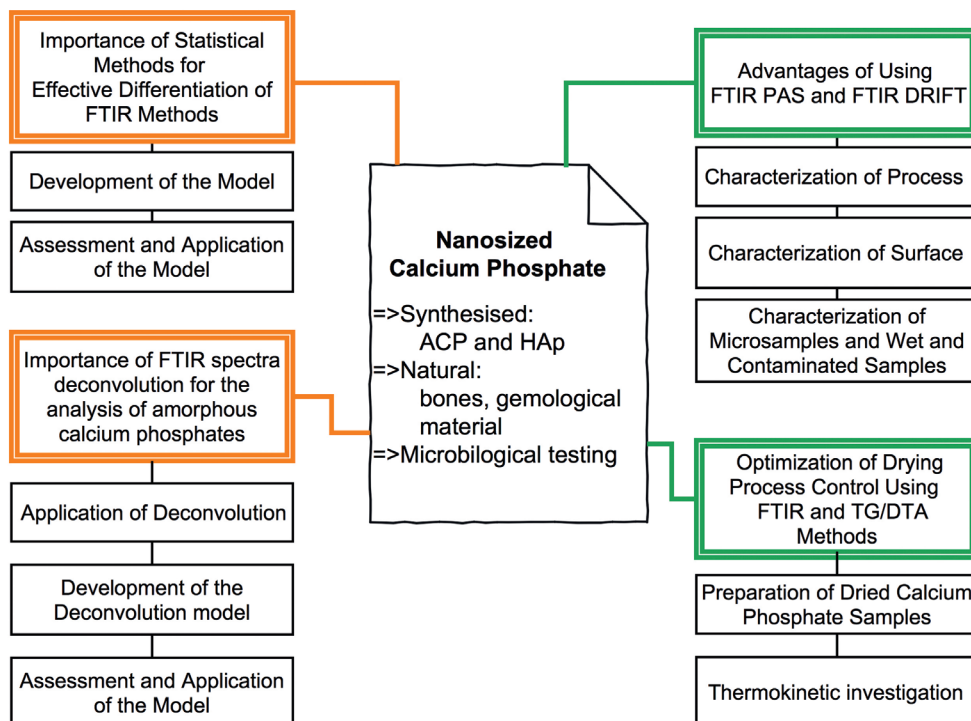


Fig. 3. The scheme of the doctoral thesis.

The following substances and materials have been selected for calcium phosphate biomaterials:

- as an inorganic form of bone, amorphous calcium phosphate (ACP) and HAp compounds containing carbonate ions, which by composition and properties are more intrinsic to the inorganic part of the bone than pure hydroxyapatite, are considered; samples have been synthesized with varying degrees of crystallinity (amorphous, microcrystalline, crystalline) and particle size (1 nm – 70 nm);
- contemporary and archeological human bones (Mesolithic Age, Neolithic Age, 15<sup>th</sup>–16<sup>th</sup>; Institute of History of Latvia);
- synthetic calcium phosphate in conjunction with a microbiological sample – *in vitro* studies.

The chemical precipitation method was used to obtain synthetic samples. Modified E. Hayek and M. Jarcho methods were used in this work, which C. Rey several times has described in his works [16], in order to obtain nanosized compounds for amorphous compounds.

The following commercial and freeware computer programs were tried out and information was gathered for FTIR spectrum processing and digital conversion: *SpekWin32 1.72*, *SpectraGryph 1.06*, *MagicPlot Student 2.5.1*, *Grams/Al*, *Origin 10*, *Simca 14*. The spectra were processed by background correction, spectrum alignment, normalization, Fourier self-deconvolution (FSD), and the second derivative.

Data statistical analysis was performed using computer programs *Origin 10*, *Simca 14*, *Statistica 10.0*.

# RESULTS AND DISCUSSION

## 1. Development and Assessment of the Comparison Model of FTIR Methods for Nanosized Calcium Phosphate Research.

### 1.1. Development of the Model for the Mutual Qualitative and Quantitative Comparison of Different FTIR Methods

One of the important tasks of FTIR was to find out if and how the FTIR spectra taken with 4 different sampling methods (PAS, DRIFT, ATR and KBr) can be compared if carbonate ions containing CP with varying degrees of crystallinity and crystalline size were used: P-1, amorphous powder substance, particle size <1nm; P-2, microcrystalline material, particle size ~ 10 nm; P-3, microcrystalline material, particle size ~ 20 nm; P-4, crystalline material, particle size ~ 70 nm. At the beginning of the study, a work plan was developed that included the process and the expected results (Fig. 4).

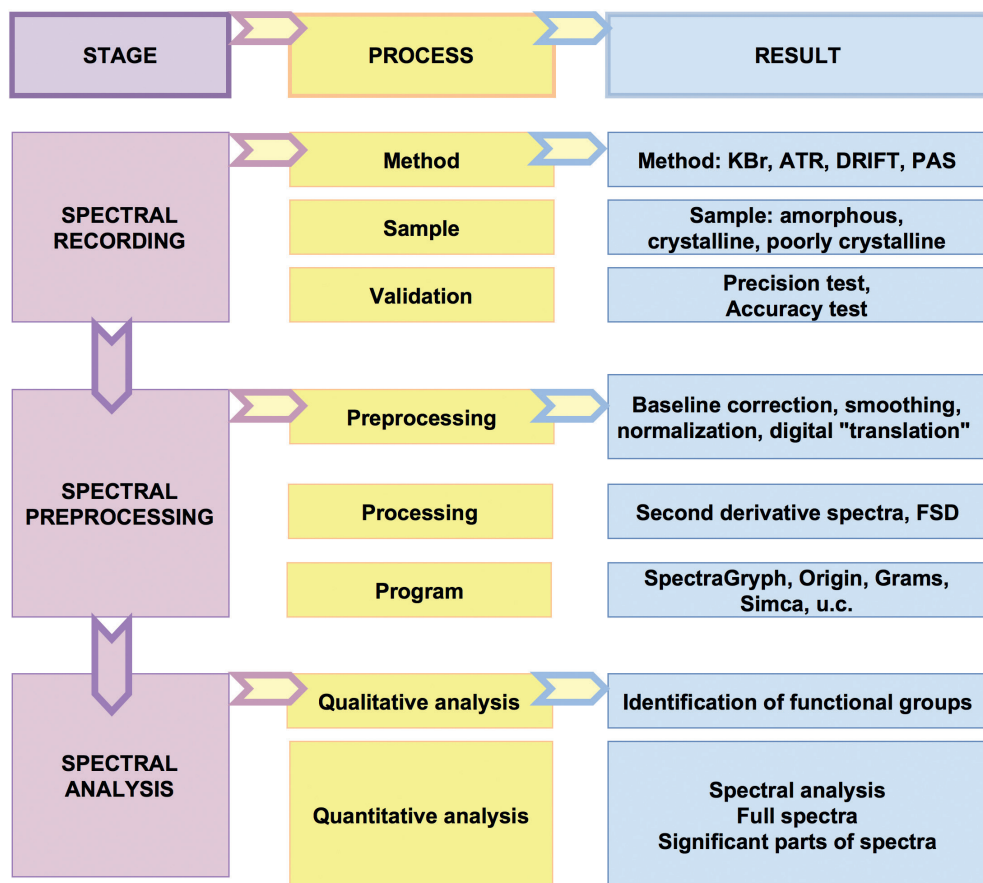


Fig. 4 The work plan for comparing different FTIR methods

## 1.2. Qualitative Analysis of FTIR Spectra

All the received spectra were initially compared qualitatively (Fig. 5). As the spectral absorption area of the ATR method is narrower than other methods, all the sampling methods were then compared in the 528–4000  $\text{cm}^{-1}$  area. Spectral “noises” were observed in both the ATR and PAS spectra in the 1950–2450  $\text{cm}^{-1}$  area. However, these “noises” did not affect the qualitative analysis of the FTIR spectra of HAP because they were located outside the analytically significant area of functional groups. All the FTIR spectra were distributed and observed in four areas (Fig. 6): *F1*\_528 – 700; *F2*\_800 – 1200; *F3*\_1350 – 1800; *F4*\_3450 – 3950. The main results are summarized in Table 1.

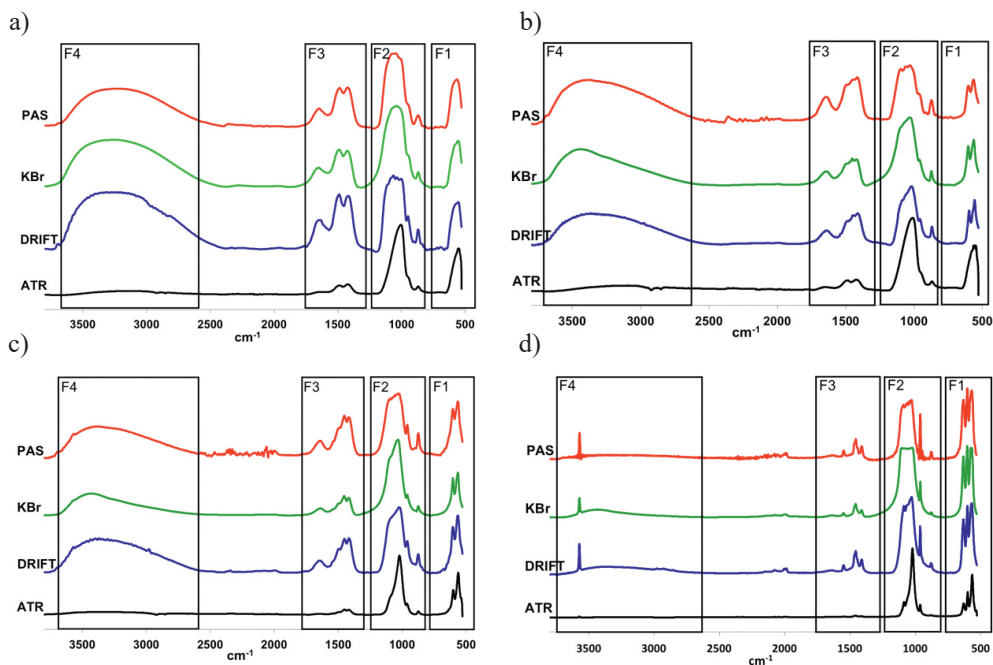


Fig. 5. FTIR spectra of four sampling methods for samples of different degrees of crystallinity and size: a) P-1-CCP particle size < 1 nm; b) P-2-CCP particle size ~ 10 nm; c) P-3-CCP particle size ~ 20 nm, d) P-4 – CCP particle size ~ 70 nm.

\* Particle size determined by XRD and program Profex3.10.2.

Visually all four FTIR sampling methods describe the spectra similarly, but there are several differences in the ATR spectra:

- 1) in the carbonate ion region, the spectra have a much lower absorption rate;
- 2) there are no visible absorption lines in the spectral area of 2450–3950  $\text{cm}^{-1}$  of the  $\text{OH}^-$  group for the microcrystalline samples;
- 3) crystalline samples have very weak absorption lines in the spectral area of 2450–3950  $\text{cm}^{-1}$  of the  $\text{OH}^-$  group;
- 4) For the amorphous and microcrystalline samples, the ATR method exhibits a very weak absorption of  $\text{H}_2\text{O}$  in the spectral area of ~ 2450–3950  $\text{cm}^{-1}$ .

Differences in ATR spectra are significant in the interpretation of calcium phosphate spectra. They indicate weak sensitivity of the method in the areas concerned. This method

Table 1

**Qualitative detection of functional groups with FTIR samples of varying degrees of crystallinity**

Spectral area, cm <sup>-1</sup>	Functional groups	P-1 Amorphous < 1nm	P-2 Microcrystalline ~10 nm	P-3 Microcrystalline ~20 nm	P-4 Crystalline ~70 nm
<i>F1</i> 450–780	$\nu_4 \text{PO}_4^{3-}$	KBr, DRIFT, PAS, ATR	KBr, DRIFT, PAS, ATR	KBr, DRIFT, PAS, ATR	KBr, DRIFT, PAS, ATR
	OH <sup>-</sup>	KBr, DRIFT, PAS, ATR	KBr, DRIFT, PAS, ATR	KBr, DRIFT, PAS, ATR	KBr, DRIFT, PAS, ATR
<i>F2</i> 800–1200	$\nu_1, \nu_3 \text{PO}_4^{3-}$ $\nu_2 \text{CO}_3^{2-}$	KBr, DRIFT, PAS, ATR	KBr, DRIFT, PAS, ATR	KBr, DRIFT, PAS, ATR	KBr, DRIFT, PAS, ATR
<i>F3</i> 1350–1800	$\nu_3 \text{CO}_3^{2-}$ A, B, non-apatitic; OH <sup>-</sup>	KBr, DRIFT, PAS, ATR (w)*	KBr, DRIFT, PAS, ATR (w)	KBr, DRIFT, PAS, ATR (v.w.)**	KBr, DRIFT, PAS, ATR (v.w.)
<i>F4</i> ~2450–3950	OH <sup>-</sup>	KBr, DRIFT, PAS, ATR (n.o.)	KBr, DRIFT, PAS, ATR (n.o.)	KBr, DRIFT, PAS, ATR (n.o.)**	KBr, DRIFT, PAS, ATR (v. w.)
	H <sub>2</sub> O	KBr, DRIFT, PAS, ATR (n. o.)	KBr, DRIFT, PAS, ATR (n.o.)	KBr, DRIFT, PAS, ATR (n.o.)	KBr (w), DRIFT (w), PAS (w), ATR (n.o.)

\* w – weak, \*\* v.w. – very weak, \*\*\* n.o. – not observed

is not applicable to the characterization of the crystallinity of calcium phosphates and the quantitative characterization of carbonate ions, which may lead to false conclusions.

### 1.3. Quantitative (statistical) Analysis of the FTIR Spectra

Combining the FTIR methods with multidimensional statistical analysis, quantitative data and conclusions about the effect of spectrum processing on the obtained results were obtained; all FTIR spectra were analyzed both in their full length FULL (528–4000 cm<sup>-1</sup>) and in constrained areas: CUT (528–700 cm<sup>-1</sup> ( $\nu_4 \text{PO}_4^{3-}$ , OH<sup>-</sup>), 800–1200 cm<sup>-1</sup> ( $\nu_1$  and  $\nu_3 \text{PO}_4^{3-}$ ,  $\nu_2 \text{CO}_3^{2-}$ ), 1350–1800 cm<sup>-1</sup> ( $\nu_3 \text{CO}_3^{2-}$  A, B, non-apatitic; OH<sup>-</sup>)), and in certain areas of the functional groups F1, F2, F3, F4 (areas of the functional groups see Fig. 5).

Various spectrum processing methods were evaluated: baseline correction (L), normalization (N) and background correction (F), and Fourier self-deconvolution method (FSD). The 2nd derivative (2DER) was applied to the processed spectra. The study compared the processed spectra with and without the 2nd order derivative. The samples were coded according to the processing methods: *Processing\_FN*, *Processing\_FNL*, *Processing\_FNL\_FSD*, *Processing\_FN\_2DER*, *Processing\_FNL\_2DER*, *Processing\_FNL\_FSD\_2DER*.

The following statistical methods were used in the work: Pearson Correlation Coefficients (PKK), Principal Component Analysis (PCA) and Hierarchical Cluster Analysis (HCA).

For PKK calculations, spectra were compared to FTIR KBr, because it is the most commonly used method for both qualitative and quantitative studies of calcium phosphates and is considered to be the most appropriate measure [6], [7]. All the correlations obtained are reliable if  $|r| > r_{0,05;24}$ . For PCA analysis, the largest variances were shown by the first

two components (PC1 and PC2), so their variances and cumulative dispersion are discussed in the following chapters. All component calculation methods have a confidence level of 95 %. The formation of clusters was depicted in diagrams and dendograms. The Ward's Principle of Similarity and the Euclidean Distance Method were used in the preparation of the dendograms.

#### **Full Spectrum Area – FULL (528–4000 cm<sup>-1</sup>).**

**Pearson coefficients.** The ATR method shows a 30–40 % lower PKK values (0.508 against DRIFT, 0.642 against KBr, 0.688 against PAS) than DRIFT or PAS against KBr. The correlation coefficients are  $< 0.750$  ( $|r| > r_{0.05;24}$ ), which indicates a moderate correlation. The values of the Pearson coefficients for the ATR spectra of amorphous samples P-1 depend on the spectrum processing method. They are slightly lower than for the crystalline samples. The derivatives of the spectra show a sharp decline in PKK values. For instance, *Processing\_FNL\_2DER* ( $< 0.550$ ) and with *Processing\_FNL\_FSD\_2DER* ( $< 0.300$ ), which indicates a very weak correlation but opens the way for differentiation of samples.

The value of the Pearson coefficient for the ATR spectra of crystalline samples P-4 does not depend on the spectrum processing method, since very similar values of the Pearson correlation coefficient for all processing methods are presented. The Pearson correlation coefficients are  $> 0.750$  ( $|r| > r_{0.05;24}$ ), which indicates a close correlation. The derived spectra of crystalline samples also show a decrease in PKK values. However, this drop is similar to all processing methods.

In the analysis of the Principal Components, PC variances are influenced by the spectrum processing method.

For non-derived processed spectra, PC1 variances are greater than those processed with 2nd order derivatives. For derived spectra, the effect of the PC1 variance reduces, but the impact of PC2 and each subsequent PC increases; the cumulative values for the sum of PC1 and PC2 decrease, indicating the effect of the next major component, such as PC3, PC4. This opens the way for differentiation of more similar spectra, for less the analytically insignificant part (background, “noises”) of the spectrum is taken into account. The total cumulative dispersion is formed by 90 % when two main components are created for non-derivative spectra and in some cases even 5–7 clusters for derived spectra (see Table 2).

Table 2

**Variances and cumulative dispersion of major components by the modes of spectrum processing in the area FULL (528–4000 cm<sup>-1</sup>)**

<b>Mode of spectrum processing</b>	<b>Variances of PC1 and PC2, %</b>	<b>Total cumulative dispersion, %</b>
Processing_FN	PC1(68.4) + PC2 (16.4)	84.8
Processing_FNL	PC1(88.8) + PC2 (4.0)	92.9
Processing_FNL_FSD	PC1(86.7) + PC2 (5.0)	91.8
Processing_FNL_2DER	PC1(58.7) + PC2 (21.0)	79.7
Processing_2DER	PC1(50.6) + PC2 (14.4)	65.0
Processing_FNL_FSD_2DER	PC1(58.5) + PC2 (12.8)	71.3

\* confidence level 95 %

Cluster analysis using 2D diagrams. The spectra selection used is homogeneous, the probability of cluster formation is influenced by the spectrum processing method (Fig. 6). For the ATR method, the location of samples in clusters is significantly different from the location for the other three FTIR methods, often outside the range of significance of 95 % or joins other clusters, or forms separate clusters for the ATR method. This leads to the conclusion that cluster formation is not affected by the choice of the FTIR method, except when choosing the ATR method (for instance, Fig. 6b, 6c). For non-derived processed spectra, regardless of the type of spectrum processing, a clear cluster formation is not observed (e.g., Fig. 6a).

The derived spectra show a pronounced formation of 2–3 clusters (see Fig. 6b, 6c) according to the degree of crystallization and particle size.

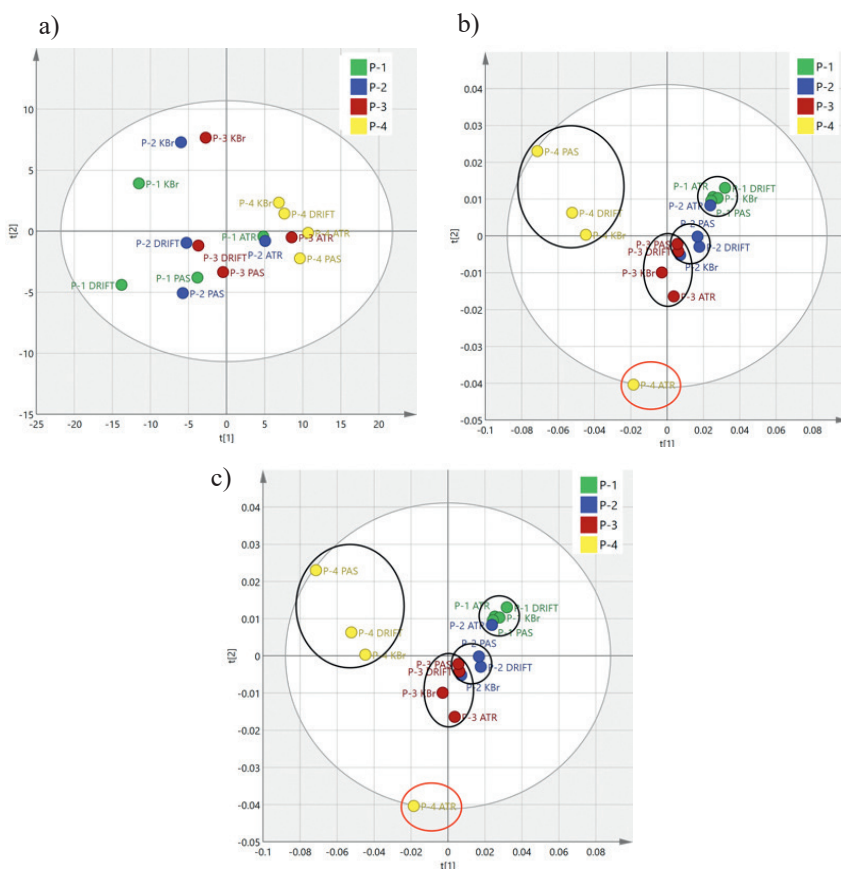


Fig. 6. Cluster formation for processed spectra by 4 FTIR methods in the full spectrum area depending on the processing method: a) *Processing\_FNL*; b) *Processing\_FNL\_2DER*; c) *Processing\_FNL\_FSD\_2DER*.

- The crystalline P-4 sample cluster is most evident in all cases considered. This leads to the conclusion that the degree of crystallization plays a crucial role in cluster formation and its effect on the form of a spectrum is sufficient to be used for research.

- A common cluster of microcrystalline samples P-2 and P-3. Since the particle size of the sample is very similar, it is possible to divide these samples into separate clusters only if the spectrum is processed by *Processing\_FNL\_FSD\_2DER* or, in the statistical analysis, only 3 spectra of FTIR methods (KBr, DRIFT and PAS, excluding significantly different ATR) are used, or only areas of separate functional groups (Fig. 7a).

The cluster of the amorphous sample P-1 overlaps with the clusters of microcrystalline samples P-2 and P-3 on several occasions (for instance, Fig. 6b, 6c). However, it is possible to isolate this cluster, if the spectrum is processed by *Processing\_FNL\_FSD\_2DER* and only spectra processed by 3 FTIR methods (KBr, DRIFT and PAS) are used in the statistical analysis (Fig. 7a).

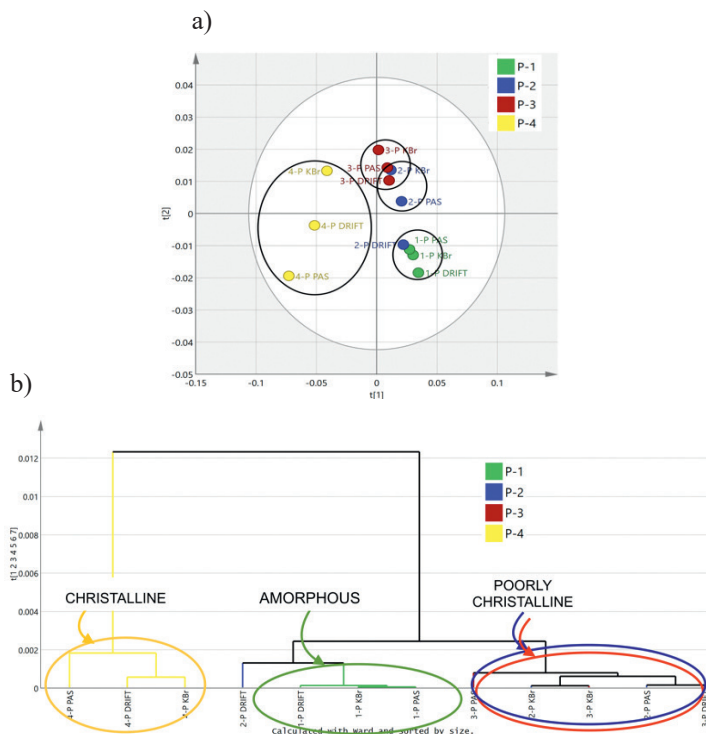


Fig. 7. a) Cluster formation for the spectra processed by three FTIR methods in the full spectrum area with *Processing\_FNL\_FSD\_2DER*; b) HCA analysis for the spectra processed by three FTIR methods in the full spectrum area with *Processing\_FNL\_FSD\_2DER*.

In the cluster analysis, using dendrograms, the clusters are most clearly formed for the processed derived spectra (for instance, Fig. 7a), similarly to the methods discussed above. The analysis shows that the greatest influence on cluster formation is not the choice of the FTIR method, but the degree of crystallinity of the sample and the size of the particles. This is most accurately indicated in diagrams without the ATR method (for instance, Fig. 7b).

Narrowing the research areas, leaving only analytically significant areas, for instance, **F1** (528 – 700  $\text{cm}^{-1}$  ( $\nu_4 \text{PO}_4^{3-}$ , OH $^-$ ), **F2** 800 – 1200  $\text{cm}^{-1}$  ( $\nu_1$  and  $\nu_3 \text{PO}_4^{3-}$ ,  $\nu_2 \text{CO}_3^{2-}$ ), **F3** 1350 – 1800  $\text{cm}^{-1}$  ( $\nu_3 \text{CO}_3^{2-}$  A, B, non-apatitic OH $^-$ ) the following information was obtained.

Pearson coefficients. PKK increases by about 20–30 %. It is  $> 0.850$  ( $|r| > r_{0.05;24}$ ). The correlation is very close. The highest correlation coefficients ( $> 0.920$ ), irrespective of the degree of crystallization and the processing of spectra, are shown by the carbonate area: 1350–1800  $\text{cm}^{-1}$  ( $\nu_3 \text{CO}_3^{2-}$  A, B, non-apatitic;  $\text{OH}^-$ ). For the derived spectra of the amorphous samples, the values of PKK decrease by 40–50 %, while for the crystalline ones only about 20 %. The low values of PKK for amorphous and microcrystalline samples enable the samples to be differentiated.

Analysis of main components. A significant decrease of the PCI variance and an increase of the effect of subsequent components PC2, etc. are observed for the processed spectra by the second order derivative (see Table 3).

Table 3

**Variations and cumulative dispersion of the main components by the modes of spectrum processing in the area of  $\text{F3}_{1350 - 1800 \text{ cm}^{-1}}$  ( $\nu_3 \text{CO}_3^{2-}$  A, B, non-apatitic;  $\text{OH}^-$ )**

Mode of spectrum processing	Variations of PC1 and PC2, %	Total cumulative dispersion, %
Processing_FN	PC1(93.1) + PC2 (4.8)	97.9
Processing_FNL	PC1(97.1) + PC2 (14.5)	98.6
Processing_FNL_FSD	PC1(96.6) + PC2 (14.7)	98.0
Processing_FN_2DER	PC1(55.6) + PC2 (21.8)	77.4
Processing_2DER	PC1(46.8) + PC2 (21.2)	67.9
Processing_FNL_FSD_2DER	PC1(50.7) + PC2 (22.3)	73.0

\* confidence level 95 %

The 2D diagram of cluster analysis and the dendrogram for the three FTIR methods demonstrate (Fig. 8a, 8b) that the main effect in cluster formation is directly the particle size and degree of crystallinity.

- For amorphous and microcrystalline samples, the method of spectrum processing plays an important role in differentiating samples. It is best to differentiate the processed spectra with the 2nd order derivative.
- The higher the degree of crystallinity of the sample, the more similar are the spectra of all four methods, and less results are affected by the method of spectrum processing.

## Conclusions

- The Pearson coefficients, analysis of the main components and analysis of clusters confirm the results obtained by analyzing qualitatively the spectra of 4 FTIR sampling methods for samples of varying degrees of crystallinity.
- The values of PKK for the ATR method and the location in clusters differ significantly from other FTIR methods.
- The methods of FTIR DRIFT, PAS and KBr show a close correlation, therefore it can be concluded that the choice of method has little effect on the differentiation of nanosized calcium phosphates.
- The method of spectrum processing influences the possibility of sample differentiation: clusters are most clearly formed by derivatizing the processed spectra.

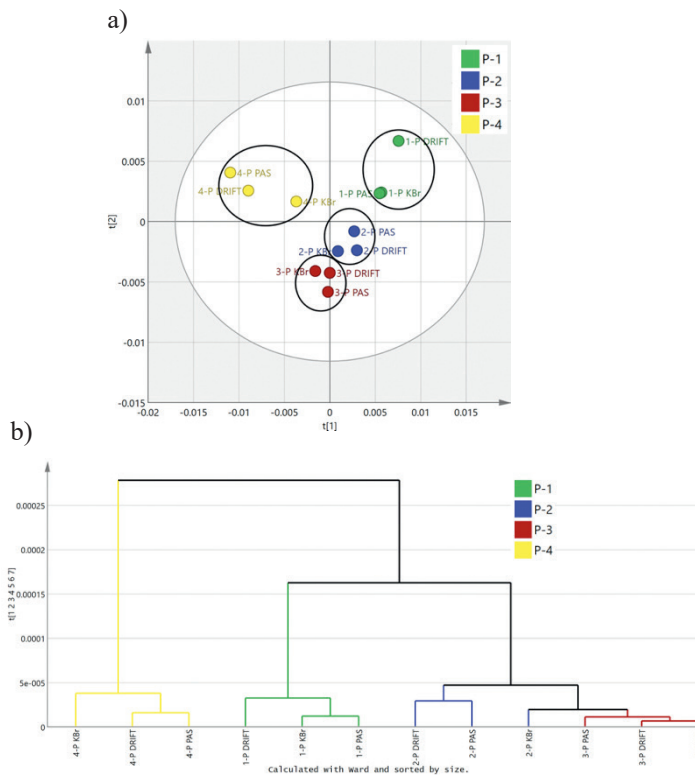


Fig. 8. a) Cluster formation for the processed spectra by three FTIR methods: in the area of  $F3\ 1350\text{--}1800$  with *Processing\_FNL\_FSD\_2DER*; b) Cluster formation for the processed spectra by the three FTIR methods: in the area of  $F3\ 1350\text{--}1800$  with *Processing\_FNL\_FSD\_2DER*.

- Most importantly, the degree of crystallization and the particle size affect the differentiation of the samples: the clusters are most clearly formed by narrowing spectral areas of the processed derived spectrum to the areas of functional groups.

The information obtained in the study can be used for the development of a research model and for differentiation of unknown samples.

To summarize the information obtained, a scheme was developed for choosing FTIR methods and spectrum processing and analyzing, which shows the main steps from taking a FTIR spectrum to the conclusion (see Appendix 1).

#### 1.4. Model Assessment and Usage Options

**Development of the model.** The closest correlations were observed by classifying the samples according to the degree of crystallization of the substance and the particle size. Therefore, when approbating the model, it was assumed that the visual interpretation of FTIR spectra allows us to predict the result to be achieved, as there is a strong correlation between the spectral visual image in the area of  $450\text{--}750\ \text{cm}^{-1}$  ( $\nu_4\ \text{PO}_4^{3-}$ ,  $\text{OH}^-$ ), visualization of crystallite dimensions and data in the 2D PC1, PC2 diagrams, and the cluster HCA dendrograms (Fig. 9).

1. Amorphous samples with the particle size  $< 5$  nm have one wide spike in the area of ( $\nu_4 \text{PO}_4^{3-}$ ) and they will form a common cluster in the PC and HCA diagrams.
2. Microcrystalline samples with the particle size of 5 nm to 30 nm have two bands in the area of ( $\nu_4 \text{PO}_4^{3-}$ ) and they will form a common cluster in the PC and HCA diagrams.
3. Crystalline samples of the particle size  $> 30$  nm have three bands in the area of ( $\nu_4 \text{PO}_4^{3-}$ ) and they will form a common cluster in the PCA and HCA diagrams.

**Assessment of the model.** The standard substances of calcium phosphate with varying degrees of crystallinity and particle size were used: amorphous ( $\sim 1$  nm), microcrystalline (10 nm) and two crystalline samples (60 nm and 70 nm).

- To increase the number of measurements, 10 samples of nanosized calcium phosphate powder containing carbonate ions with varying degrees of crystallization and particle size were selected.
- The method of the work was FTIR-DRIFT and for comparison – XRD and Rietveld analysis.
- The method for spectrum processing was *Processing\_FNL\_2DER*.

**Model analysis.** The assumption about sample placement in clusters was confirmed, because samples created clusters with standards at the marked points.

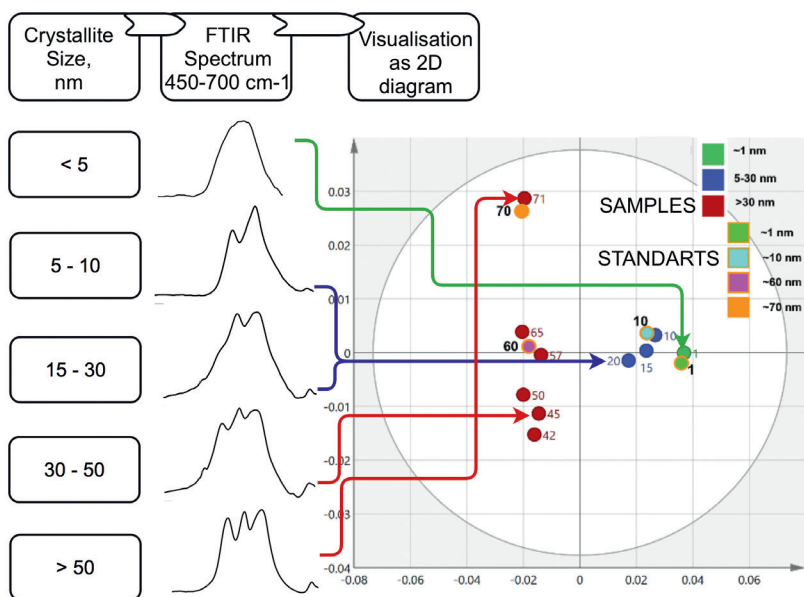


Fig. 9. Relationships of FTIR visual interpretation and statistical analysis for determining the crystallinity and particle size of calcium phosphate.

For the processed spectra in the full spectrum area 3 clusters were formed according to the particle size and crystallinity (Fig. 10a). The obtained data were confirmed by the HCA dendrogram (Fig. 10b), since it was evident that two distinct clusters were formed: one for completely crystalline samples and the other for amorphous and microcrystalline samples, which in turn formed two less different clusters.

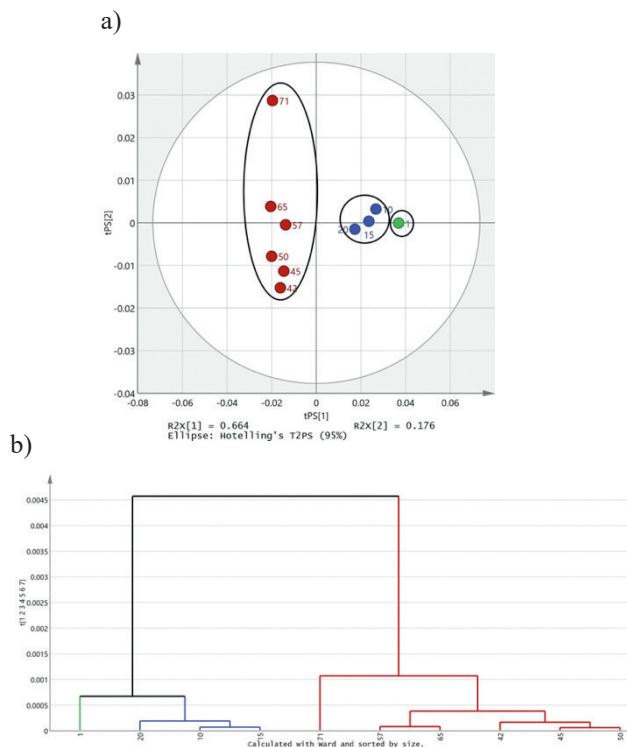


Fig. 10. Appropriation of the model in the full spectrum area for samples of different degrees of crystallinity and particle size: a) 2D diagram with PC1 and PC2; b) HCA.

The sample of the particle size 71 is located in a common cluster with the samples of the particle size greater than 30 nm. It can be seen that the samples of particle size greater than or equal to 70 nm could form a separate cluster, but studies in this direction were not continued.

Continuing assessment of the model in selected areas of functional groups, it showed that clusters were formed in all analytically significant areas of calcium phosphate: 450–700  $\text{cm}^{-1}$  ( $\nu_4 \text{PO}_4^{3-}$ ,  $\text{OH}^-$ ), 800–880 ( $\nu_3 \text{CO}_3^{2-}$ ), 900–1200  $\text{cm}^{-1}$  ( $\nu_1 \nu_3 \text{PO}_4^{3-}$ ), 1350–1800  $\text{cm}^{-1}$  ( $\nu_3 \text{CO}_3^{2-}$  A, B, non-apatitic;  $\text{OH}^-$ ) (Fig. 11).

Judging by 2D diagrams, the cluster is most clearly expressed in the areas of F1 450–700  $\text{cm}^{-1}$  ( $\nu_4 \text{PO}_4^{3-}$ ,  $\text{OH}^-$ ) and F4 1350–1800  $\text{cm}^{-1}$  ( $\nu_3 \text{CO}_3^{2-}$  A, B, non-apatitic;  $\text{OH}^-$ ), which are also most often used to determine the degree of crystallinity and composition of the sample.

In the dendrograms of the areas of F1 450–700  $\text{cm}^{-1}$  ( $\nu_4 \text{PO}_4^{3-}$ ,  $\text{OH}^-$ ) and F3 900–1200  $\text{cm}^{-1}$  ( $\nu_1 \nu_3 \text{PO}_4^{3-}$ ), it can be observed that the samples of  $> 70$  nm can form a separate cluster. Similarly, in dendrograms of functional groups, it can be observed that it is possible to differentiate between amorphous and microcrystalline samples (Fig. 11).

## Conclusions

Approbation of the model confirms that the developed model, which includes the selection of samples of varying degrees of crystallinity and sizes up to 100 nm, and the spectrum processing method with the 2nd derivative, can be successfully used:

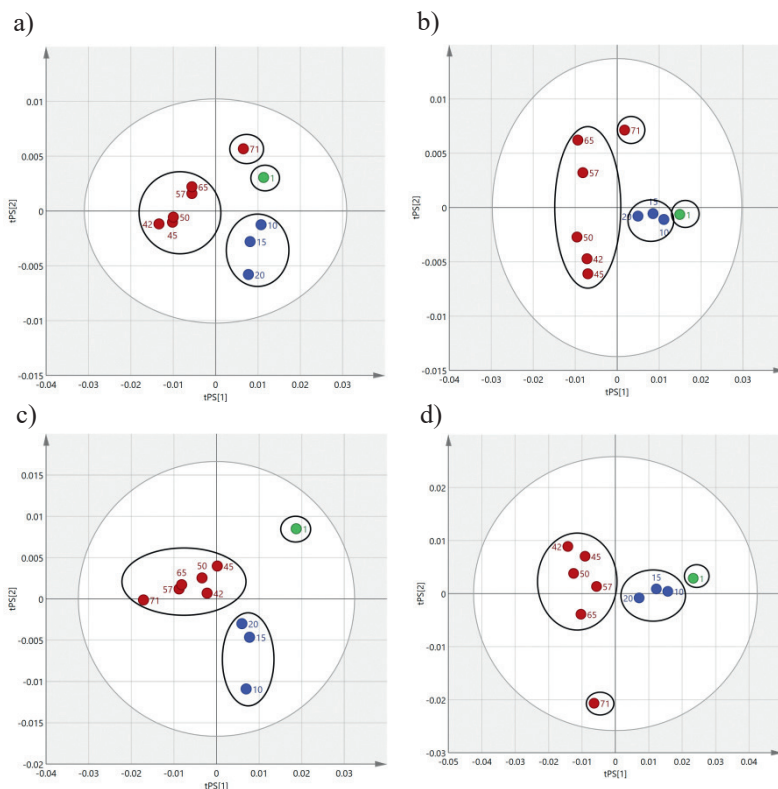


Fig. 11. Cluster formation in separate functional groups: a) 800–880 ( $\nu_3$   $\text{CO}_3^{2-}$ ); b) 1350–1800  $\text{cm}^{-1}$  ( $\nu_3$   $\text{CO}_3^{2-}$  A, B, non-apatitic;  $\text{OH}^-$ ); c) 450–700  $\text{cm}^{-1}$  ( $\nu_4$   $\text{PO}_4^{3-}$ ,  $\text{OH}^-$ ); d) 900–1200  $\text{cm}^{-1}$  ( $\nu_1$   $\nu_3$   $\text{PO}_4^{3-}$ ).

- 1) for approximate evaluation of crystalline size and degree of crystallization (amorphous, microcrystalline, crystalline) in the sample, without using XRD and Rietveld methods;
- 2) by the visual image of the FTIR spectrum in the area of 450–700  $\text{cm}^{-1}$  ( $\nu_4$   $\text{PO}_4^{3-}$ ,  $\text{OH}^-$ ), it is possible to predict the position of the sample in the cluster and crystallite parameters (size and degree of crystallinity);
- 3) the PC and HCA analysis helps to confirm or rule out assumptions and evaluate the effects of factors on cluster formation.

## 2. Thermokinetic Studies of Nanosized Calcium Phosphate

In order to subject the substance to the effects of temperature, it is necessary to obtain information on its thermal stability. In the process of production, calcium phosphates undergo heat treatment several times by drying, calcining and sintering. Temperature affects calcium phosphates, both their phase and degree of crystallinity, and particle size may change. Similarly, the effect of temperature on amorphous calcium phosphates containing carbonate ions is observed in the following FTIR spectral areas: 400–700  $\text{cm}^{-1}$  ( $\nu_4$   $\text{PO}_4^{3-}$ ,  $\text{OH}^-$ ), 800–950  $\text{cm}^{-1}$  ( $\nu_2$   $\text{CO}_3^{2-}$ ), 1350–1800  $\text{cm}^{-1}$  ( $\nu_3$   $\text{CO}_3^{2-}$  A, B, non-apatitic;  $\text{OH}^-$ ) and 3450–3950  $\text{cm}^{-1}$  ( $\text{H}_2\text{O}$ ;  $\text{OH}^-$ ).

## 2.1. Optimization of Drying Process Control

The main task was to study both the stability of the amorphous phase and change of physically and chemically bound water in the process of drying. The FTIR DRIFT, FTIR PAS and DTA / TG methods were used to study the process.

First, the drying process of a freshly filtered ACP was studied using FTIR spectroscopy. FTIR spectroscopy allows to observe vibrations of the O-H bond that depend on the strength and length of the hydrogen bond, measurement temperature, and other factors.

When taking FTIR PAS spectra for filtered precipitate (see Fig. 12), significant changes in the FTIR spectrum are already seen in the early hours. In the first hours, the main changes occur in the spectral areas of  $3450\text{--}3950\text{ cm}^{-1}$  ( $\text{H}_2\text{O}$ ;  $\text{OH}^-$ ) and  $1640\text{ cm}^{-1}$  and only after 24 h, in the spectrum it is possible to observe a spike formation characteristic of apatite in the area of  $400\text{--}700\text{ cm}^{-1}$  ( $\nu_4\text{ PO}_4^{3-}$ ,  $\text{OH}^-$ ) and  $1350\text{--}1800\text{ cm}^{-1}$  ( $\nu_3\text{ CO}_3^{2-}$  A, B, non-apatitic).

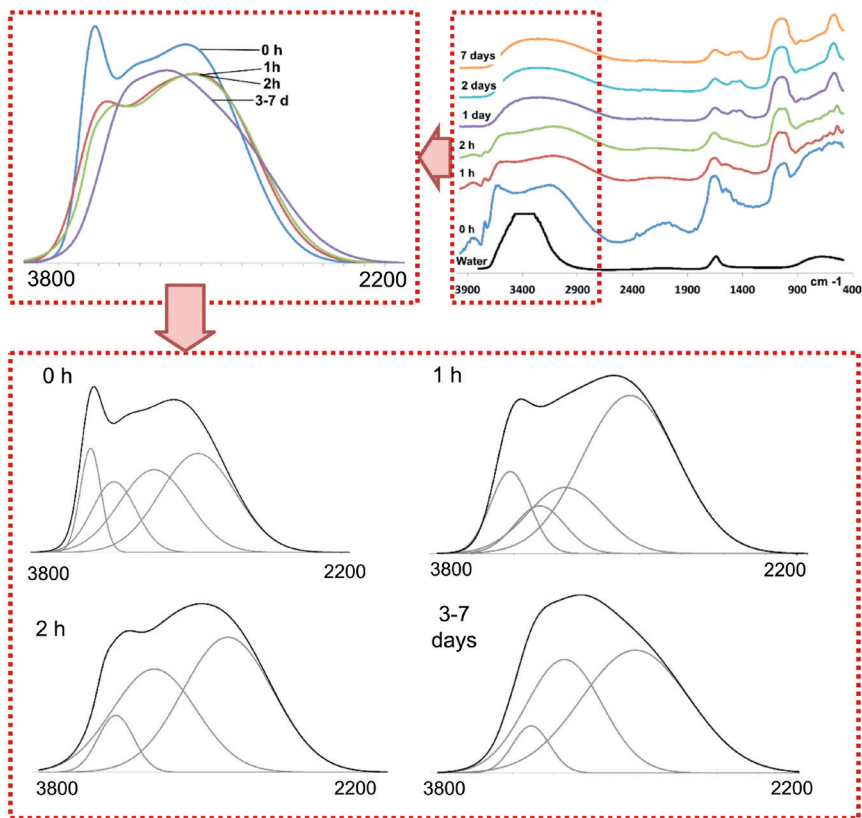


Fig. 12. CACP drying kinetics, drying in air

\* The FTIR PAS method was used to measure kinetics

More detailed information on changes in water and OH groups can be obtained by deconvolution of the spectral area from  $2200\text{ to }3800\text{ cm}^{-1}$ . Comparing the given areas, one can see a change of the form at the time (Fig. 12).

When deconvoluting it is possible to find out four water-specific bands at 3020, 3272, 3488 and 3622  $\text{cm}^{-1}$  that are initially visible, which over time “shift”, blend in and form the  $\text{H}_2\text{O}$  / OH absorption lines characteristic of the amorphous calcium phosphate (Fig. 12). Rapid changes in the FTIR spectrum indicate that initially a large amount of water is only physically absorbed on the surface and large amount of energy is not required to remove it.

In this work, the ACP containing carbonate ions were studied, which were dried under various conditions: lyophilized, 25 °C, 50 °C, 80 °C, ethanol/25 °C, acetone/25 °C, 120 °C and 130 °C and retained the amorphous or microcrystalline structure after drying.

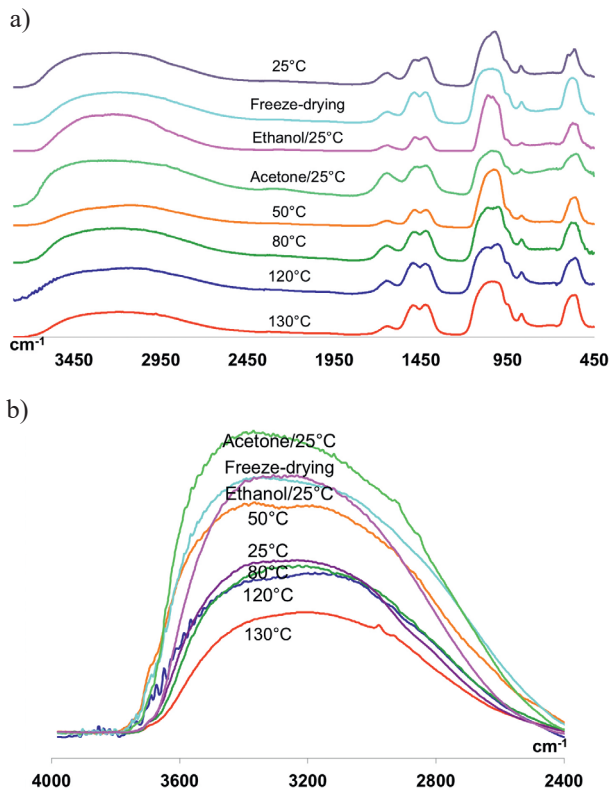


Fig. 13. The FTIR DRIFT spectra of dried CACP: a) in the full spectral area; b) in the area of 3800–2000  $\text{cm}^{-1}$ .

In the FTIR PAS spectra, in the area of 2400–4000  $\text{cm}^{-1}$ , decreasing absorption intensities could be observed depending on the drying temperature (Fig. 13). The correlation was observed – the higher the drying temperature, the lower was the intensity of the bonds. Different intensities were also observed for the air-dried samples – if the sample was washed with an organic solvent (ethanol or acetone) before drying, the intensities were higher than that of the normal air-dried sample. The observed changes were related to the desorption of physically bound and bound water during the drying process.

The TG / DTA method was chosen as the main method in the study because FTIR and XRD methods did not give answers to two questions.

1. Are there any significant differences between differently dried amorphous samples?

2. Under which drying conditions, CACP loses physically bound water, but still preserves chemically bound water?

Looking at the thermograms of dried samples under different conditions in the range of 25 °C to 1000 °C, one exothermic area and one endothermic area are visible for all samples. Further in the work, only the endothermic peak will be considered, because it is related to the main water loss in the samples of calcium phosphate (Fig. 14a).

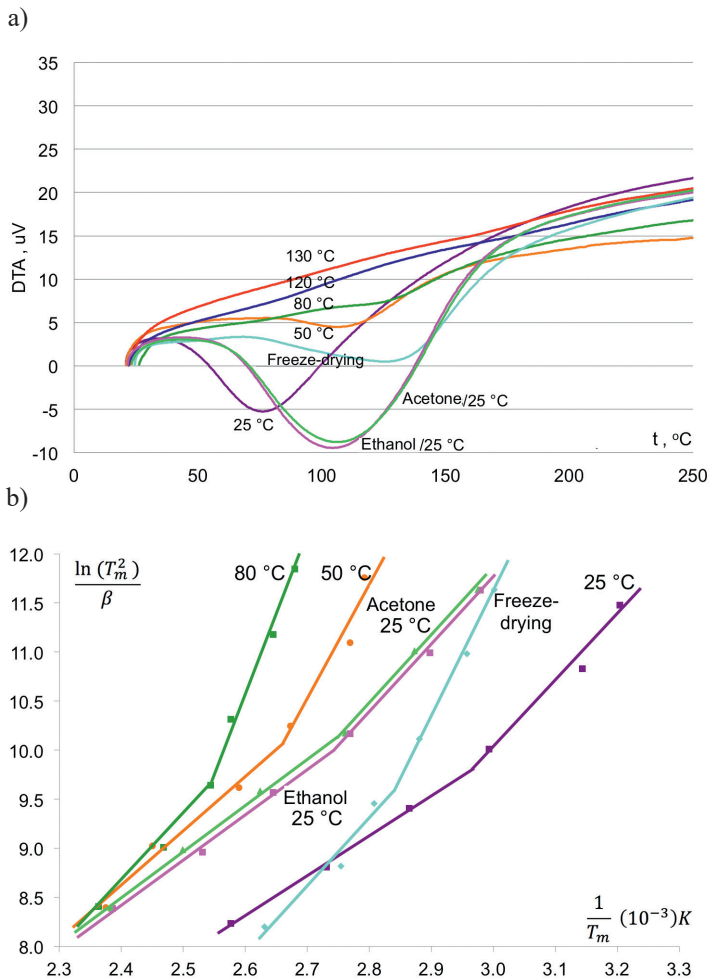


Fig. 14. DTA of calcium phosphate: a) the endothermic bands for differently dried samples. The heating rate in both figures is 10  $^{\circ}\text{C}/\text{min}$ ; b) The Arrhenius plots for amorphous calcium phosphate, where  $\beta$  is the drying rate, but  $T_m$  is the minimal temperature determined by DTA at the minimum of the endothermic plot.

In the temperature range from 25  $^{\circ}\text{C}$  to 150  $^{\circ}\text{C}$ , for the samples dried at 25  $^{\circ}\text{C}$ , 50  $^{\circ}\text{C}$ , 80  $^{\circ}\text{C}$ , ethanol / 25  $^{\circ}\text{C}$ , acetone / 25  $^{\circ}\text{C}$ , the endothermic peak is expressed, for the lyophilized sample it is weaker. But at 120  $^{\circ}\text{C}$  and 130  $^{\circ}\text{C}$  endothermic bands are not practically observed, except for the sample at 120  $^{\circ}\text{C}$  and the heating rate of 40  $^{\circ}\text{C} / \text{min}$ . In the DTA thermograms for differently dried samples at the same TG loading rate of 10  $^{\circ}\text{C} / \text{min}$ ., there

are different temperatures at the endothermic peak. For instance, 25 °C ( $T_{\min} = 71 \pm 4$  °C), 50 °C ( $T_{\min} = 105 \pm 5$  °C), 80 °C ( $T_{\min} = 122 \pm 5$  °C), ethanol/25 °C ( $T_{\min} = 103 \pm 5$  °C), acetone/25 °C ( $T_{\min} = 105 \pm 5$  °C).

For physically and chemically bound water analysis, activation energy and critical temperatures were calculated by Ozawa-Flynn-Wall and Kissinger methods and Arrhenius graphs were plotted (Fig. 14b). Each graph consists of two straight lines (bottom line – the gradient of the physically sorbed water, and the upper line – the gradient of the chemically sorbed water) that intersect at the point of inflection. At the point of inflection, the critical temperature can be determined when the physically sorbed water is released and chemically sorbed water begins to release.

Although for all the samples studied, the visual FTIR spectra and diffractograms were very similar, calculations showed different values of critical temperatures of activation energy of the samples for the release of physically and chemically bound water (Table 4).

For the air-dried samples (both usually dried and solvent-treated),  $T_{\text{crit}}$  and  $E_a$  show lower values than the lyophilized and treated at 50 °C to 80 °C samples, which shows a higher stability of these samples in the subsequent storage (Table 4).

Table 4

**The critical temperatures and values of activation energy of dried amorphous samples**

Parameters	Air	Lyophilization	50 °C	80 °C	Ethanol/ air	Acetone/ air
$T_{\text{crit}}$ , °C	64±3	86±4	103±4	124±5	91±4	84±5
$E_a$ (phys.), kJ/mol	34±1	59±2	49±2	57±2	38±1	41±1
$E_a$ (chem.) kJ/mol	54±2	100±4	92±4	120±5	57±2	57±2

When analyzing the TG graphs, the samples show different mass losses at the end of the heating process at 1200 °C. Differences in mass loss can be observed at the very beginning of the heating process (Fig. 15).

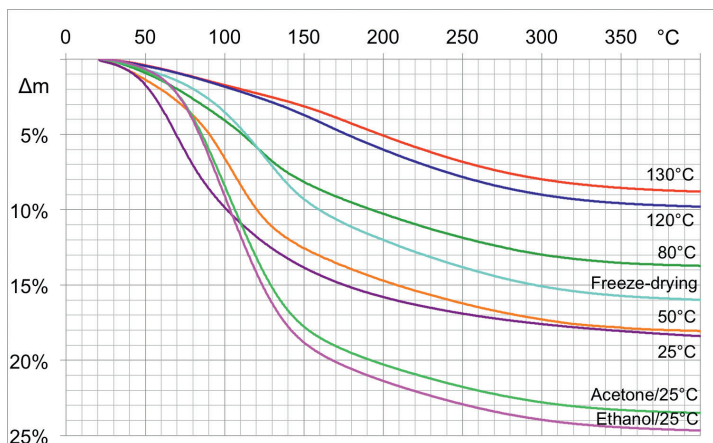


Fig. 15. TG graphs for differently dried amorphous calcium phosphates.

The main differences for all samples in the mass loss were observed before and after  $T_{\text{crit}}$  (see Table 5). Up to 200 °C, the greatest loss of mass was for the samples treated with an

organic solvent. This could be explained by solvent contamination not only on the surface of the sample but also in the structure and by the trend of hydrophilic solvents to create azeotropic mixtures which, when heated, are released at higher temperatures than of pure solvents.

Mass spectrometry was used to demonstrate the presence of solvents. The mass spectra clearly showed (Fig. 16) that when drying the sample at the room temperature it is not possible to get rid of organic solvents ethanol and acetone.

All the studied samples showed similar mass losses at the temperature of 200–650 °C, which could be explained by the fact that only chemically sorbed water has remained in all the studied samples and the basic structure is similar in all the samples. Differences in mass loss at 650 °C can be explained by the different location of carbonate ions in the structure of calcium phosphate. The location of carbonate ions in the structure under the influence of temperature is described in the next chapter.

Table 5

**Mass loss at different temperatures for dried amorphous samples**

Parameters	Air	Lyophilization	50 °C	80 °C	Ethanol/air	Acetone/air	120 °C	130 °C
$\Delta m$ %, $T_{crit}$	1.5±0.2	2.6±0.3	7.1±0.4	6.2±0.4	8.0±0.4	4.7±0.3	3.2±0.3	2.4±0.3
$\Delta m$ %, $T_{crit-200}$	9.6±0.5	6.7±0.4	8.2±0.4	4.3±0.3	14.0±0.6	15.7±0.7	4.4±0.3	2.6±0.3
$\Delta m$ %, $T_{200-600}$	4.1±0.3	4.6±0.3	5.0±0.3	4.7±0.3	5.7±0.3	5.4±0.3	5.4±0.3	5.0±0.3
$\Delta m$ %, $T_{600-650}$	0.2±0.05	0.2±0.05	0.3±0.05	0.2±0.05	0.5±0.1	0.5±0.1	0.4±0.1	0.4±0.1
$\Delta m$ %, $T_{650-1000}$	3.4±0.3	1.0±0.1	0.8±0.1	0.7±0.1	2.1±0.2	1.6±0.2	2.1±0.2	2.1±0.2
$\Delta m$ %, $T_{20-1000}$	17.6±0.9	14.3±0.7	19.8±1.0	15.3±0.8	27.3±1.3	25.6±1.3	14.7±0.8	11.9±0.6

## Conclusions

1. The drying technology of the substances has a critical effect on the structure of the substance and the degree of moisture.
2. The usage of organic solvents in the drying process of substances is not desirable, as solvents are thus involved in the structure and may affect their usage for biomedical purposes.
3. Evaporation of water from the samples is observed up to 600 °C, indicating its close binding with the structure of the substance;

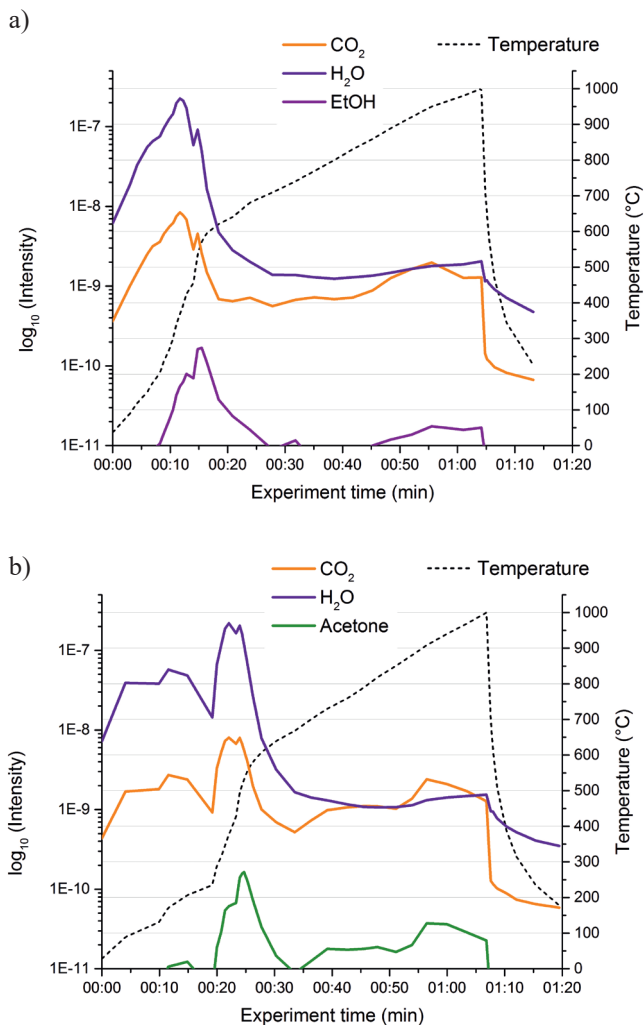


Fig. 16. The mass spectra for the samples washed with a) ethanol and b) acetone.

- The release of  $\text{CO}_2$  and  $\text{H}_2\text{O}$  is observed throughout the drying process, even up to 600  $^{\circ}\text{C}$ , indicating a change in the structure of the substance rather than a simple loss of moisture, as it was previously thought to be a sequential process for the release of  $\text{H}_2\text{O}$  and  $\text{CO}_2$ .

## 2.2. Changes in Content of Carbonate Ions Due to Temperature

The area of carbonate ions was studied because their composition and location may change in the structure of calcium phosphate due to temperature: A-type  $\text{CO}_3^{2-}$ , B-type  $\text{CO}_3^{2-}$  or non-apatitic  $\text{CO}_3^{2-}$  (see Table 6). The aim of the study: using deconvolution to analyze how the location of carbonate ions changes in the structure during the drying and calcining process.

In this chapter, the FTIR DRIFT spectral areas of carbonate ions were studied (see Fig. 17):  $800\text{--}950\text{ cm}^{-1}$  ( $\nu_2\text{ CO}_3^{2-}$ ) and  $1350\text{--}1800\text{ cm}^{-1}$  ( $\nu_3\text{ CO}_3^{2-}$  A, B, non-apatitic;  $\text{OH}^-$ ). Two samples were selected from the series with different degrees of crystallinity, particle size and the content of carbonate ions obtained by drying and heating the samples under different conditions. All the samples after XRD and Rietveld analysis were divided into 3 groups: amorphous (sample A), microcrystalline (B–D) and crystalline (E–J).

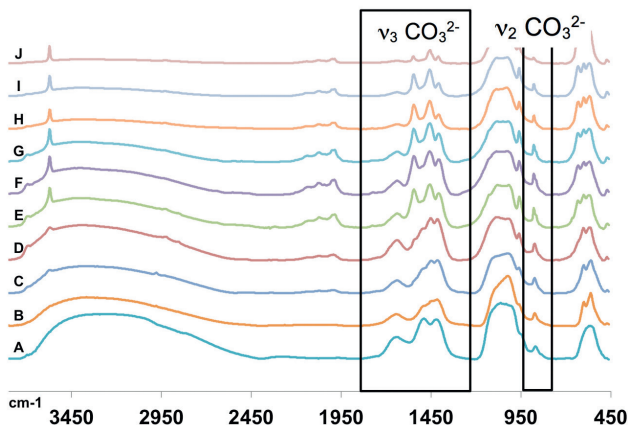


Fig. 17. The FTIR DRIFT spectra of the change of the composition of carbonate ions due to temperature in the full area where A – lyophilized, B –  $80\text{ }^\circ\text{C}/4\text{h}$ , C –  $200\text{ }^\circ\text{C}$ , D –  $300\text{ }^\circ\text{C}$ , E –  $700\text{ }^\circ\text{C}/10\text{ min}$ , F –  $700\text{ }^\circ\text{C}/30\text{min}$ , G –  $700\text{ }^\circ\text{C}/50\text{ min}$ , H –  $800\text{ }^\circ\text{C}/20\text{ min}$ , I –  $800\text{ }^\circ\text{C}/40\text{ min}$ , J –  $900\text{ }^\circ\text{C}/20\text{min}$ .

In the study, the presence of carbonate ions was visually detected from the FTIR spectra in their entire area and the structure of their A and B carbonates was roughly estimated. This was possible because the functional groups indicated in the literature were used. Although in the FTIR spectrum the bands of carbonate ions overlap, it can be concluded that the maximums of B bands dominate at lower values of  $\text{cm}^{-1}$ , but the areas of A bands at higher values of  $\text{cm}^{-1}$  (Fig. 17). The pronounced composition of B-carbonates is visible for amorphous samples and predominates for microcrystalline samples, but the composition of A-carbonates entirely for crystalline samples.

The method of deconvolution was used to obtain detailed information.

The deconvolution of the area of  $\nu_2\text{ CO}_3^{2-}$  demonstrates that:

- B-  $\text{CO}_3^{2-}$  vibrations are characteristic in the amorphous sample (Fig. 18a);
- in the microcrystalline samples (Fig. 18b), the carbonate composition can be very different, even of all three types of carbonate (B-  $\text{CO}_3^{2-}$ , A-  $\text{CO}_3^{2-}$  and non-apatitic);
- in the crystalline samples (Fig. 18d), the content of A- $\text{CO}_3^{2-}$  carbonates predominates, but the presence of B- $\text{CO}_3^{2-}$  can also be detected. For instance, by deconvoluting Sample E, a pronounced formation of the spike of A-carbonate can be observed and it is possible to conclude the minimum time and temperature to form a pronounced spike of A-carbonate. When deconvoluting Sample J (Fig. 18d), it can be concluded that the heating conditions of  $900\text{ }^\circ\text{C}$  for 20 min. are not enough to completely replace B- $\text{CO}_3^{2-}$  structure with A- $\text{CO}_3^{2-}$  structure.

The deconvolution provides the ability to track if the desired sample structure has been achieved during the heating process. The deconvolution in the area of  $\nu_2$   $\text{CO}_3^{2-}$  is summarized in Fig. 18.

The deconvolution of the area of  $\nu_3$   $\text{CO}_3^{2-}$  shows that:

- in the amorphous sample B- $\text{CO}_3^{2-}$  vibrations are characteristic (Fig. 19a);
- in the microcrystalline samples (Fig. 19b, d, the carbonate composition can be very different, for instance, B- $\text{CO}_3^{2-}$  or even two types (B- $\text{CO}_3^{2-}$ , non-apatitic). Deconvolution provides the ability to trace changes of the carbonate type even in relatively small ranges of temperature;
- in the crystalline samples (Fig. 19d), the type A- $\text{CO}_3^{2-}$  predominates in the composition of carbonates, but the presence of B- $\text{CO}_3^{2-}$  can also be detected. The change of carbonate type from B- $\text{CO}_3^{2-}$  to A- $\text{CO}_3^{2-}$  can be detected in the samples heated even for relatively short periods of time, for instance, in Sample E heated at 700 °C for only 10 min., the presence of both A and B carbonates can be detected.

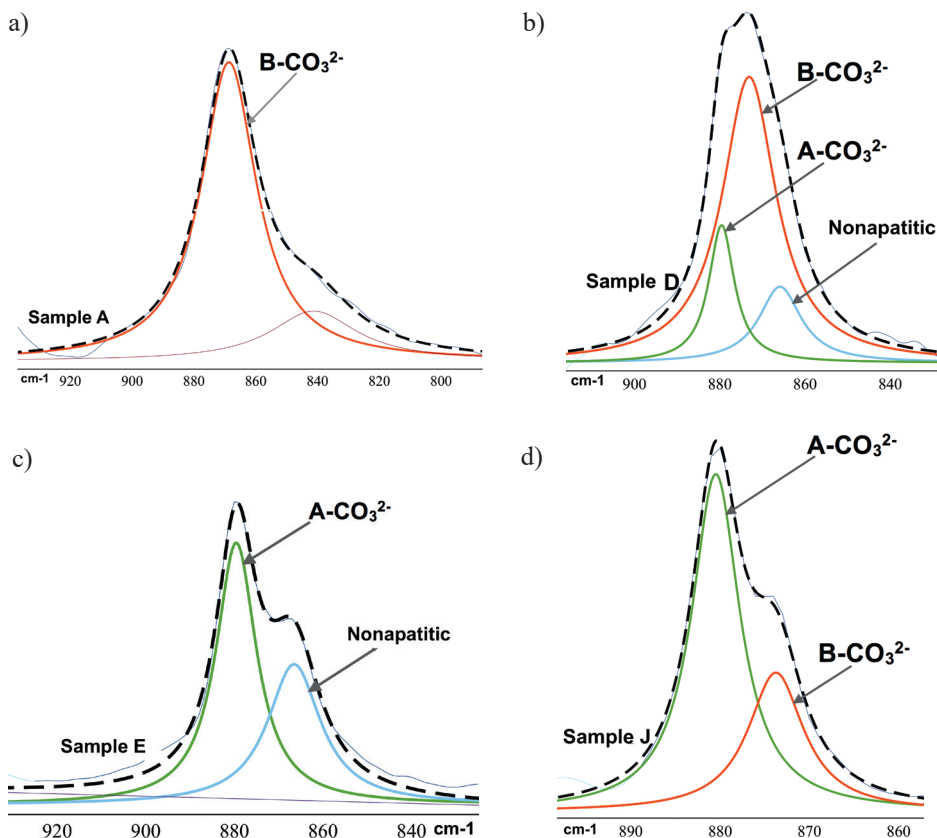


Fig. 18. The area of  $\nu_2$  of  $\text{CO}_3$  bonds (800–920  $\text{cm}^{-1}$ ): A – lyophilized, B – 80 °C/4h, D – 300 °C, E – 700 °C/10min., J – 900 °C/20min.

The deconvolution in the area of  $\nu_3$   $\text{CO}_3^{2-}$  is summarized in Fig. 19.

### Methodical recommendations for deconvolution

As a result of the study, methodological recommendations for the **deconvolution** of FTIR spectra in the area of carbonate ions were developed, which is more fully covered in the full text dissertation.

### Conclusions

Deconvoluting the spectra both in the area of  $\nu_2$   $\text{CO}_3^{2-}$  and  $\nu_3$   $\text{CO}_3^{2-}$ , the following conclusions were formulated.

1. Composition and structure of carbonates depend on the temperature and the heating time.
2. When heated, it is possible to change the type of carbonates in the structure of the sample from type  $\text{B-CO}_3^{2-}$  to type  $\text{A-CO}_3^{2-}$ .

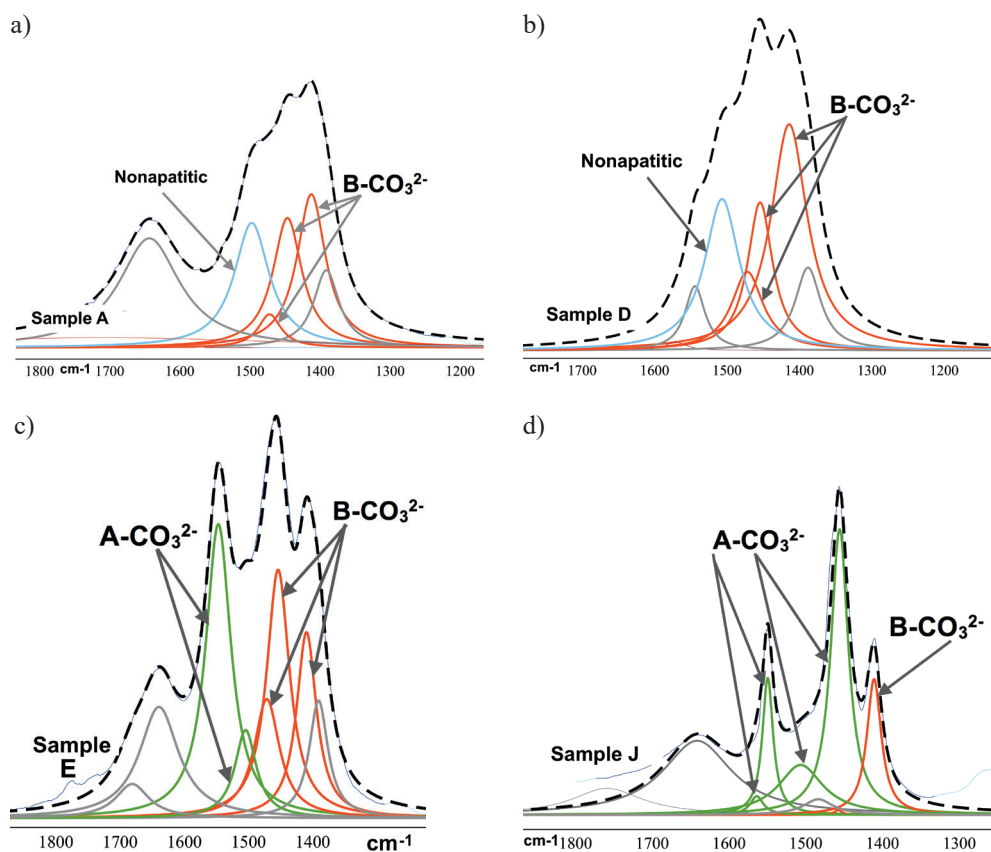


Fig. 19. The area of  $\nu_2$  of  $\text{CO}_3$  bonds  $\nu_3$   $\text{CO}_3$  (1350 – 1800  $\text{cm}^{-1}$ ): A – lyophilized, B – 80 °C/4h, D – 300 °C, E – 700 °C/10 min., J – 900 °C/20 min.

3. In the spectra of both areas of carbonates  $\nu_2$   $\text{CO}_3^{2-}$  and  $\nu_3$   $\text{CO}_3^{2-}$ , the composition of carbonates is similar:
  - a) the structure of B- $\text{CO}_3^{2-}$  dominates for the amorphous samples (Figs. 18 and 19, Sample A);
  - b) For the microcrystalline samples, the type of carbonates is temperature dependent. The structure may contain only B- $\text{CO}_3^{2-}$  and simultaneously both A- $\text{CO}_3^{2-}$  and B- $\text{CO}_3^{2-}$  or even all three carbonate structures (A, B and non-apatitic structure) (Figs. 19 and 20, Samples B and D);
  - c) In the crystalline samples there is a sharp increase in the intensity of A- $\text{CO}_3^{2-}$  and a decrease in the intensity of B- $\text{CO}_3^{2-}$  spike.
4. The deconvolution method allows tracking changes of the structure of carbonates even at relatively small temperature intervals, both qualitatively and quantitatively, so it can be used to purposefully synthesize samples with a selected composition of carbonates.

The obtained results correlate with the FTIR study model developed in the previous chapter and the results of statistical analysis (Figs. 9–12).

On the basis of the above conclusions, a schematic diagram of Fig. 20 was developed, which depicts the relationships between the visual interpretation of FTIR spectra and statistical analysis for calcium phosphates with different particle size, degree of crystallinity and carbonate content. The created scheme in Fig. 20 shows that in the visual images of FTIR spectra in the areas of  $\nu_2$   $\text{CO}_3^{2-}$ ,  $\nu_3$   $\text{CO}_3^{2-}$ , the location of the sample in the cluster, a degree of crystallization (amorphous, microcrystalline, and crystalline) and the carbonate type in the structure can be related.

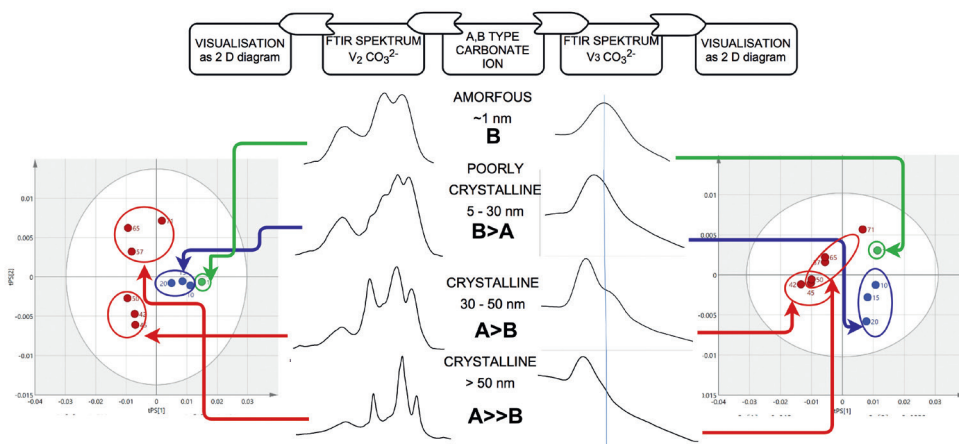


Fig. 20. The relationships of FTIR visual interaction and statistical analysis for determination of degree of crystallinity and particle size of calcium phosphate and carbonate content.

### 3. Development and Approbation of the Deconvolution Model

#### 3.1. Development of the Deconvolution Model

The deconvolution of the spectrum of human bone is necessary to better understand the structure and composition of bones and to synthesize materials of similar composition and structure (Fig. 21).

In the process of planning of the deconvolution model, the following factors were taken into account.

1. The dense bone tissue of the adult contains about 30 % of organic substances, 60 % of inorganic substances and 10 % of water. The organic substances are mainly proteins, 90 % of which are protein collagen molecules [26], but inorganic substances are mainly hydroxyapatite containing about 7 % of carbonate ions [14].
2. The amide vibrations and specific vibrations of functional groups for hydroxylapatite containing carbonate ions are characteristic of the FTIR spectra of bones.
3. The structure of hydroxyapatite in bones is microcrystalline.

In the planning process, information was gathered on bonding vibrations of both amides and carbonate ions in hydroxyapatite, and the FTIR DRIFT spectra of both the modern human bone and microcrystalline hydroxyapatite containing carbonate ions were taken (see Fig. 21).

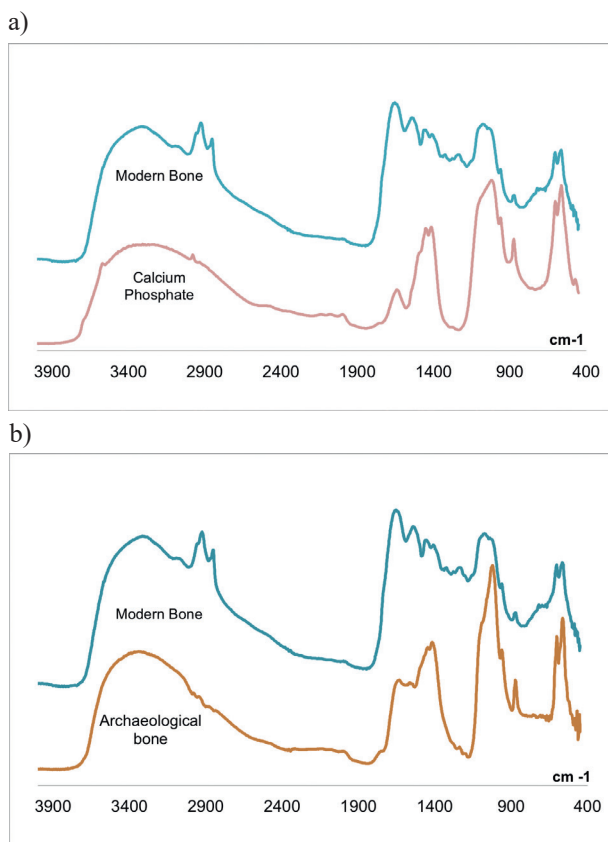


Fig. 21. The spectra of human bone and synthetic calcium phosphate: a) modern human bone and calcium phosphate; b) modern human bone and Archaeological (Mesolithic) bone.

The development of the deconvolution model was based on the use of FTIR DRIFT spectrum of modern human bone of the spectral area of 1000–2000  $\text{cm}^{-1}$  (Fig. 21). It contained the amide-specific bond positions and the positions specific of carbonate ions (Fig. 22 a). According to literature data, the vibrations of amides and carbonate ions in the area of 1000–2000  $\text{cm}^{-1}$  are very close or even overlap.

To make the model more understandable, the convolution was used – merging of deconvoluted bands. Two separate areas were created: one that is specific to amide bonds and the other that is typical only of carbonate ions. The two convoluted areas were inserted back into the distributed part of FTIR DRIFT (Fig. 22b, c, d). For further studies, the model was conditionally divided: the area of organic substances (amide) (Fig. 22b) and the area of inorganic substances (carbonate) (Fig. 22c).

Combining the convoluted areas together, one can see:

- 1) the area of organic substances (amide);
- 2) the area of inorganic substances (carbonate);
- 3) the overlapping area of inorganic and organic substances (Fig. 22d).

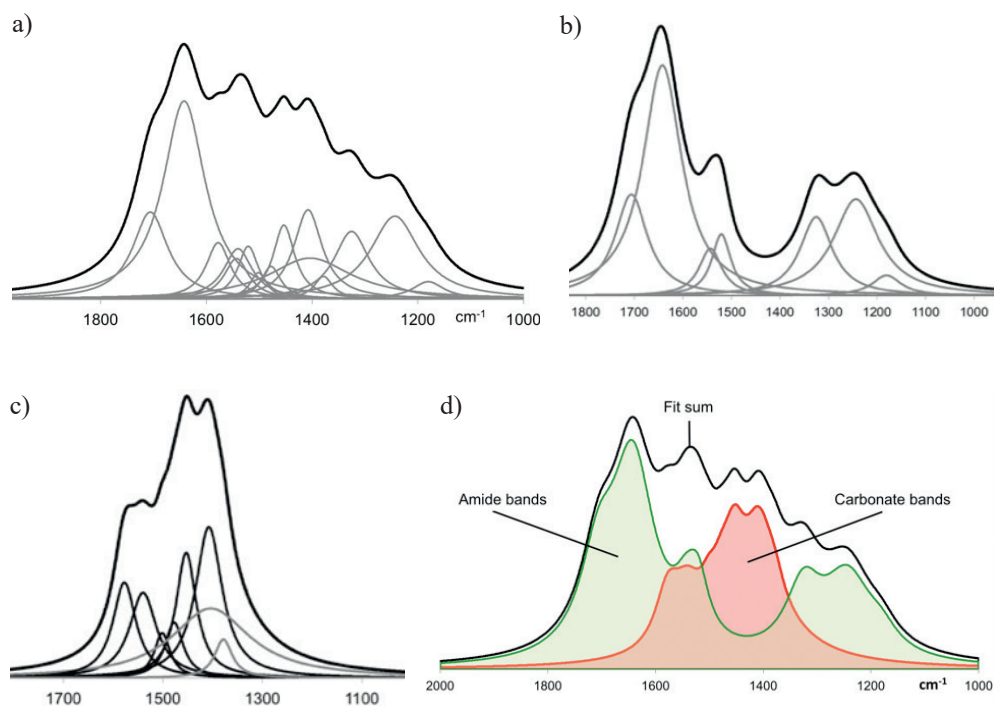


Fig. 22. The deconvoluted and convoluted modern human bone: a) the area of the deconvoluted modern human bone; b) the deconvoluted and convoluted amide area; c) the deconvoluted and convoluted area of carbonate ions; d) the convoluted modern human bone.

\* Convolution and deconvolution were carried out using free software MagicPlot Student.

### 3.2. Assessment of the Deconvolution Model

The deconvolution model was assessed using an archeological human bone and bacteria on the surface of pressed calcium phosphate.

**The archaeological study of human bone.** When visually comparing FTIR DRIFT spectrum of the archaeological bone with the spectrum of modern human bone, it can be seen that the most significant differences (Fig. 23b) are observed in the area of 1000–2000  $\text{cm}^{-1}$ . The FTIR DRIFT spectrum of the archaeological bone is similar to the spectrum of the synthesized microcrystalline calcium phosphate.

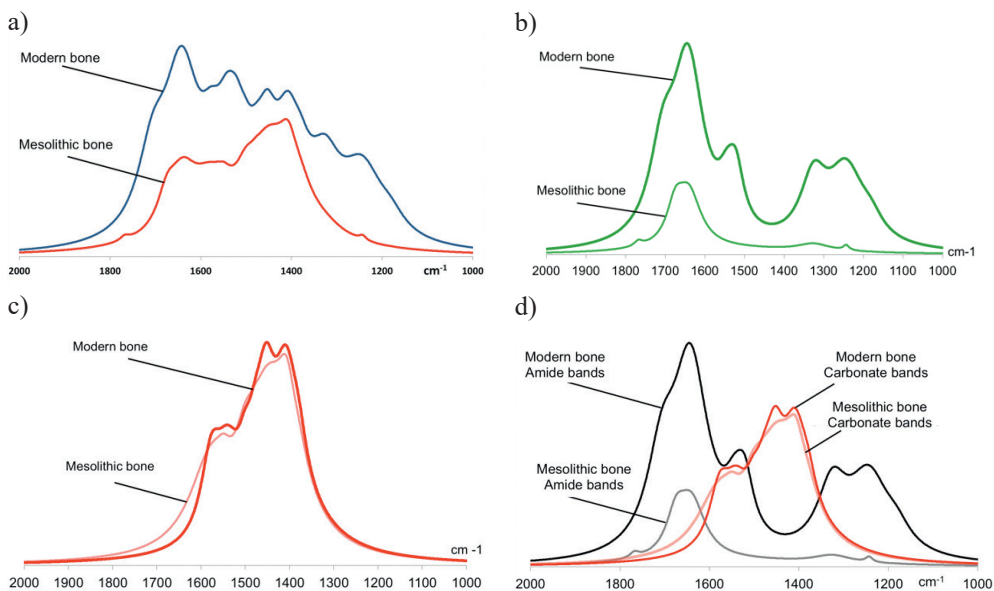


Fig. 23. The comparison of modern human bone with archaeological bone: a) FTIR DRIFT areas of 1000–2000  $\text{cm}^{-1}$ ; b) the convoluted areas of amides; c) the convoluted areas of carbonates; d) the convoluted areas of amides and carbonates.

The difference between the modern and archeological bones can be explained by the fact that the organic substances in the archeological bone were partially decomposed. To find out, the developed deconvolution model was used (Fig. 23).

### Conclusions

1. The main differences in the amide area are related to the decomposition of organic substances (proteins).
2. Small differences in the area of carbonate ions may be due to bone interactions with the soil and the environment.
3. In the given bone of the Stone Age, however, organic substances (Fig. 23d) have been preserved, which is confirmed by the presence of a small, carbonate uncovered amide peak.

## Application

1. The developed model can be used to study the structure and composition of human bones.
2. By using the developed model for archaeological bones, it is possible to determine whether organic substances have remained in the bones and whether it is expedient to send the sample for the much more expensive C-14 isotope analysis or chemical analysis.

## Qualitative Detection of Bacteria on the Surface of Pressed Calcium Phosphate

Before the experiment, it was assumed that by using FTIR PAS it is possible to simultaneously monitor two processes: changes to the surface of pressed calcium phosphate and detection of the presence of bacteria, and to observe the growth of bacteria.

The assumption was based on the following facts:

1. the FTIR PAS method is applicable not only to the study of powdered substances but also to surfaces;
2. if bacteria are placed on the surface of pressed calcium phosphate containing carbonate ions (CACP), then in the FTIR spectrum one should see both the functional groups characteristic of calcium phosphate in the areas of  $450\text{--}700\text{ cm}^{-1}$  ( $\nu_4\text{ PO}_4^{3-}$ , OH<sup>-</sup>),  $800\text{--}880$  ( $\nu_3\text{ CO}_3^{2-}$ ),  $900\text{--}1200\text{ cm}^{-1}$  ( $\nu_1\text{ } \nu_3\text{ PO}_4^{3-}$ ),  $1350\text{--}1800\text{ cm}^{-1}$  ( $\nu_3\text{ CO}_3^{2-}$  A, B, non-apatitic; OH<sup>-</sup>),  $\sim 2450\text{--}3950\text{ cm}^{-1}$  (OH, H<sub>2</sub>O), and functional groups of organic substances characteristic of bacteria. It was assumed that the main components of bacteria are carbohydrates and proteins, so in the FTIR spectrum, one should definitely see the bands characteristic of amides.

## Analysis of Spectra

1. Visually comparing the taken FTIR PAS spectra (Fig. 24a), it was found that:
  - a) for the CACP tablet, the spectrum of the surface represents the specific functional groups of calcium phosphate ( $\nu_1, \nu_3, \nu_4\text{ PO}_4^{3-}$ ,  $\nu_3\text{ CO}_3^{2-}$ ,  $\sim 2450\text{--}3950\text{ cm}^{-1}$  for OH, H<sub>2</sub>O);
  - b) the spectrum of bacteria represents the specific functional groups of bacterium *Staphylococcus epidermidis* (*S.epidermidis*) [27];
  - c) the surface of pressed CACP with bacteria depicts both the specific functional groups of bacteria and CACP.
2. Figure 25 a depicts three areas that show the main differences in the studied spectra:
  - I – area of  $1310\text{--}1200\text{ cm}^{-1}$  of the amide III bonds characteristic only of bacteria;
  - II – area characteristic of both bacteria and CACP; there is a mutual overlap of the FTIR spectra of functional groups: the spectral graphs I and II of amides in organic substances with ones of  $\nu_3\text{CO}_3^{2-}$  of A, B carbonate ions and OH in inorganic substances;
  - III – area: the characteristic absorption bands of functional groups  $-\text{CH}_3$ ,  $>\text{CH}_2$ ,  $\equiv\text{CH}$  characteristic only of bacteria.

The main differences were observed in the area of  $1200\text{--}1900\text{ cm}^{-1}$ , so this area was used for further deconvolution and analysis (Fig. 24b).

Deconvoluting and convoluting of the absorption bonds corresponding to the carbonate bonds and amide bonds in the area of  $1200\text{--}1900\text{ cm}^{-1}$ , the yield was only the spectral

characteristics of the carbonates (inorganic substances) and the spectral characteristic of the amides (organic matter) (Fig. 24c, d, e).

### Conclusions and Application

The FTIR PAS method and the developed deconvolution / convolution methodology can be used to simultaneously analyze 1) the functional groups and changes on the surface of calcium phosphate, and 2) the qualitative detection of the presence of bacteria and the bacterial reproduction process on the inorganic surface, thus evaluating the bacterial properties of the substance.

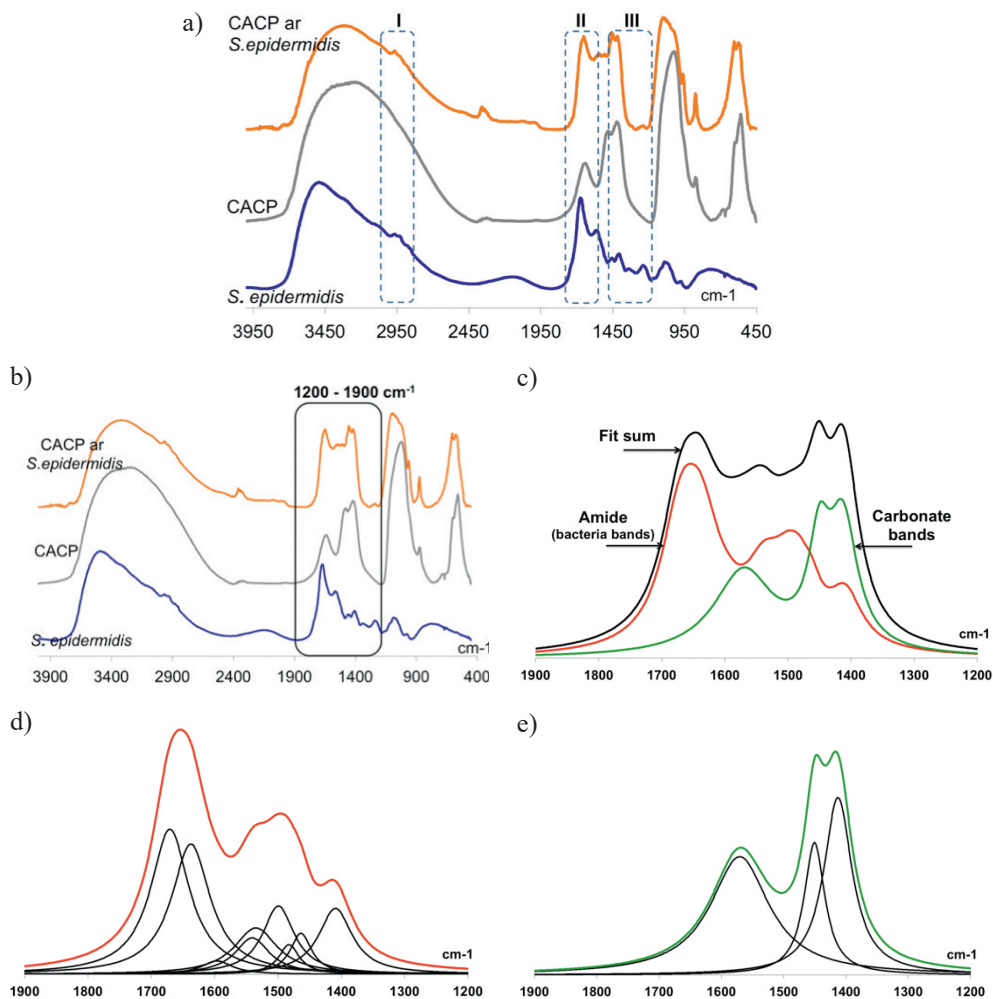


Fig. 24. FTIR PAS spectra of the surface of pressed calcium phosphate with and without bacteria: a) full spectrum with labeled distinct areas of bacteria and CACP; b) full spectrum with labeled distinct area of 1000–1900 cm<sup>-1</sup> for deconvolution; c) the convoluted area of amides and carbonates; d) the area of amides; e) the area of carbonates.

## 4. Advantages of Using PAS and DRIFT Spectroscopy in the Study of Nanosized Calcium Phosphates

### 4.1. Characterization of Microsamples

The analysis of the bone material and gemological bone materials obtained in archaeological excavations requires a non-destructive method. However, the method must be able to answer the questions about the composition, origin and authenticity of the sample. Such methods are FTIR PAS and DRIFT techniques. The following samples were used: modern human bones, human bones of archaeological excavations (the Mesolithic Age, the Neolithic Age, the 15–16th centuries) and gemological bone material.

#### Spectral Analysis

- Both methods showed bone-specific groups (Fig. 26):  $460\text{--}700\text{ cm}^{-1}$  ( $\nu_4\text{ PO}_4^{3-}$ ,  $\text{OH}^-$ ),  $900\text{--}1200\text{ cm}^{-1}$  ( $\nu_1\ \nu_3\text{ PO}_4^{3-}$ ) and the presence of  $\text{H}_2\text{O}$   $2500\text{--}3900\text{ cm}^{-1}$ . In the area of  $1000\text{--}1900\text{ cm}^{-1}$ , the amide bands characteristic of organic substances and groups of carbonate ions characteristic of inorganic substances were detected by using the deconvolution method.
- The spectra taken using both methods showed differences between the human bone spectrum and the bone material of gemological material (Fig. 25).
- The spectra taken using both methods showed differences in the spectra, depending on the place of taking the sample: the middle of the bone or the exterior of the bone.

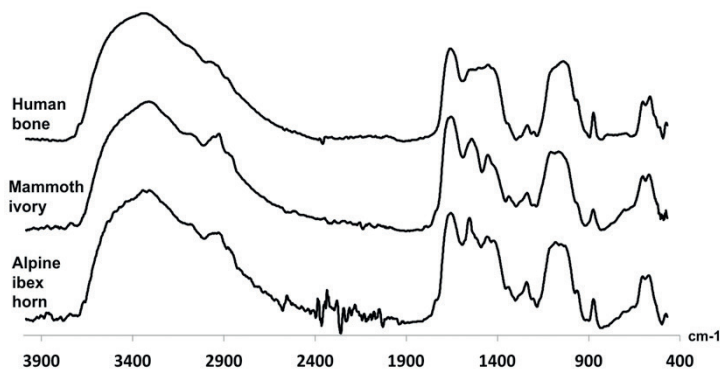


Fig. 25. The FTIR PAS of the human bone and gemological bone material.

By comparing the spectra of modern human bone and spectra of human bones from archaeological excavation using the HCA method, it was evident that there are three separate clusters for the archaeological bones and modern bone, depending on the place of taking the sample (see Fig. 26).

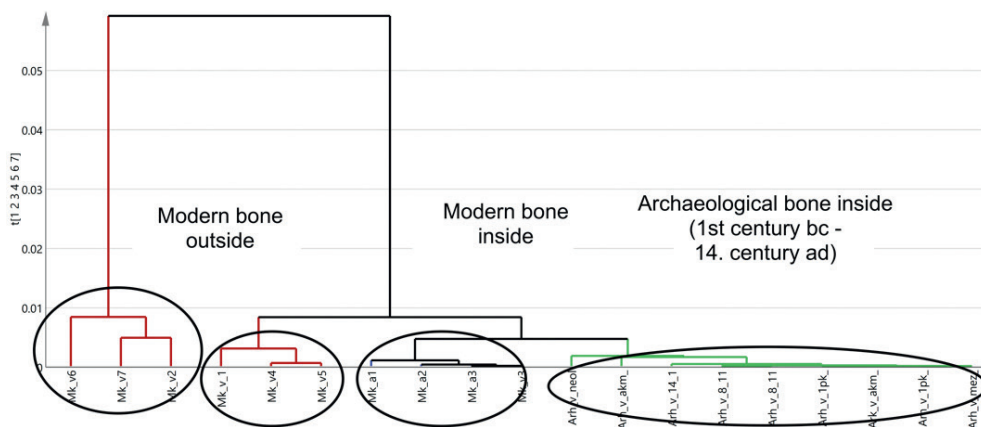


Fig. 26. The HCA dendrogram of the samples of archaeological and modern human bones using FTIR DRIFT method.

## Conclusions and Application

1. FTIR DRIFT and FTIR PAS can be used to identify bone material.
2. The material used in FTIR DRIFT and FTIR PAS method is sufficient to distinguish between
  - a) modern bone material from archeological bone material,
  - b) bone material of an animal from human bone material,
  - c) grouped samples of human bones by the place of taking the sample.
3. FTIR DRIFT can be used for analyzing the archaeological and bone material due to a small sample size as well as for analyzing valuable samples for a comprehensively quick and accurate analysis.

### 4.2. Processes in Volume

FTIR DRIFT and PAS were used to study the bacteria *Pseudomonas aeruginosa* and *Streptococcus epidermidis*. The samples were studied directly, without sample preparation.

When using FTIR DRIFT, it was observed that the bacterial sample was drying at the time on the diamond stick (see Fig. 27), therefore studies were done to determine whether the drying process has an effect on the detection and differentiation of bacteria.

## Conclusions

1. Using the analysis of the main components, it was found that FTIR DRIFT and FTIR PAS can be used successfully not only to identify the presence of bacteria but also to distinguish them (see Fig. 28).
2. FTIR DRIFT and FTIR PAS can be used successfully for the study of the drying process and crystallization process.
3. Wet samples can be used for the study without prior preparation.

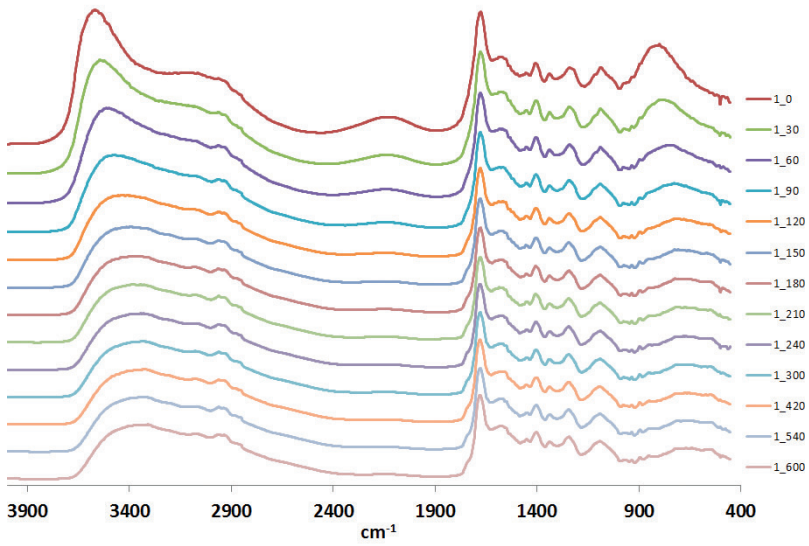


Fig. 27. FTIR DRIFT method. The drying process of bacterium *Staphylococcus epidermidis* at the time.

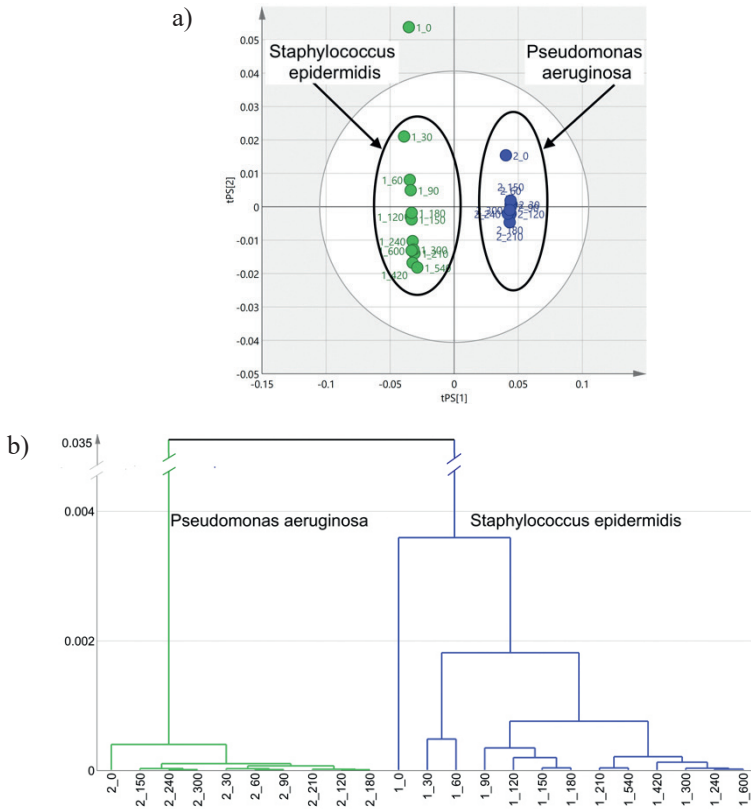


Fig. 28. The 2D PC and HCA diagrams of bacteria *Pseudomonas aeruginosa* and *Staphylococcus epidermidis*.

### 4.3. Characterization of Wet and Contaminated Samples

In order to characterize the analysis of wet samples, the method for the production of calcium phosphates was chosen as the spray-drying method because of the possibility of obtaining CCP with constant moisture content (9 %) and the contamination with nitrate and ammonium ions.

FTIR PAS spectra were taken of the samples contaminated with ammonium and nitrate ions and the pure sample.

#### Spectral analysis

1. In both FTIR spectra, vibrations of the characteristic functional groups of CCP are observed (Fig. 29).
2. In the contaminated powder, there are additional spectral graphs specific to nitrate ions and ammonium ions in the area of  $3000\text{--}3500\text{ cm}^{-1}$ ,  $2500\text{ cm}^{-1}$ ,  $1000\text{--}1500\text{ cm}^{-1}$ .

#### Conclusions and Application

1. FTIR PAS method is applicable for the analysis of wet samples, because unlike FTIR DRIFT and FTIR, KBr it does not affect the sample.
2. FTIR PAS method is sufficiently sensitive to detect slight contamination with nitrate ions and ammonium ions in the sample.
3. The quality control of wet samples allows saving at least 2 hours, which is usually spent on drying the sample.

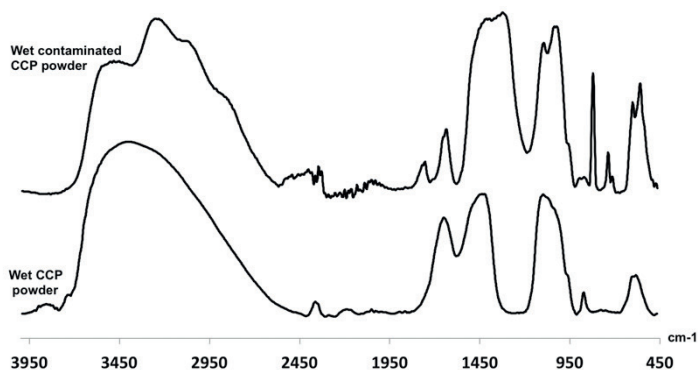


Fig. 29. FTIR DRIFT spectra of the wet contaminated and wet pure CCP sample.

### 4.4. Processes on the Surface of Calcium Phosphates

By using FTIR Spectroscopy, it is possible to analyze both calcium phosphate and bacteria. However, until now, each of these objects has been analyzed separately. This study demonstrated that by using FTIR PAS it is possible to simultaneously detect calcium phosphate-specific bonds in the area of  $460\text{--}700\text{ cm}^{-1}$  ( $\nu_4\text{ PO}_4^{3-}$ ,  $\text{OH}^-$ ),  $900\text{--}1200\text{ cm}^{-1}$  ( $\nu_1\text{ } \nu_3\text{ PO}_4^{3-}$ ) and the presence of  $\text{H}_2\text{O}$  in the area of  $2500\text{--}3900\text{ cm}^{-1}$ , and amide bonds characteristic of bacteria.

The colonized samples of bacteria *Pseudomonas aeruginosa* and *Staphylococcus epidermidis* were selected on the pressed surface of calcium phosphate.

The deconvoluted spectra allowed detecting the presence of bacteria and changes on the surface of calcium phosphate. However, it was not possible to distinguish bacteria *Pseudomonas aeruginosa* and *Staphylococcus epidermidis* one from another by using the developed methodology. The SEM method also failed to produce compelling results, since bacteria created films.

Differences between bacteria were detected using the methods for spectrum processing developed in the preceding chapters and statistical methods for bacterial FTIR PAS spectra. By performing the spectrum pre-processing and processing them with the second order derivative, the compelling clusters of *Pseudomonas aeruginosa* and *Staphylococcus epidermidis* were obtained.

Similarly, the FTIR spectra of bacteria on the surface of the pressed calcium phosphate were processed (derived and processed by the statistics). The obtained results convincingly belonged to the previously formed clusters (Figs. 30 and 31).

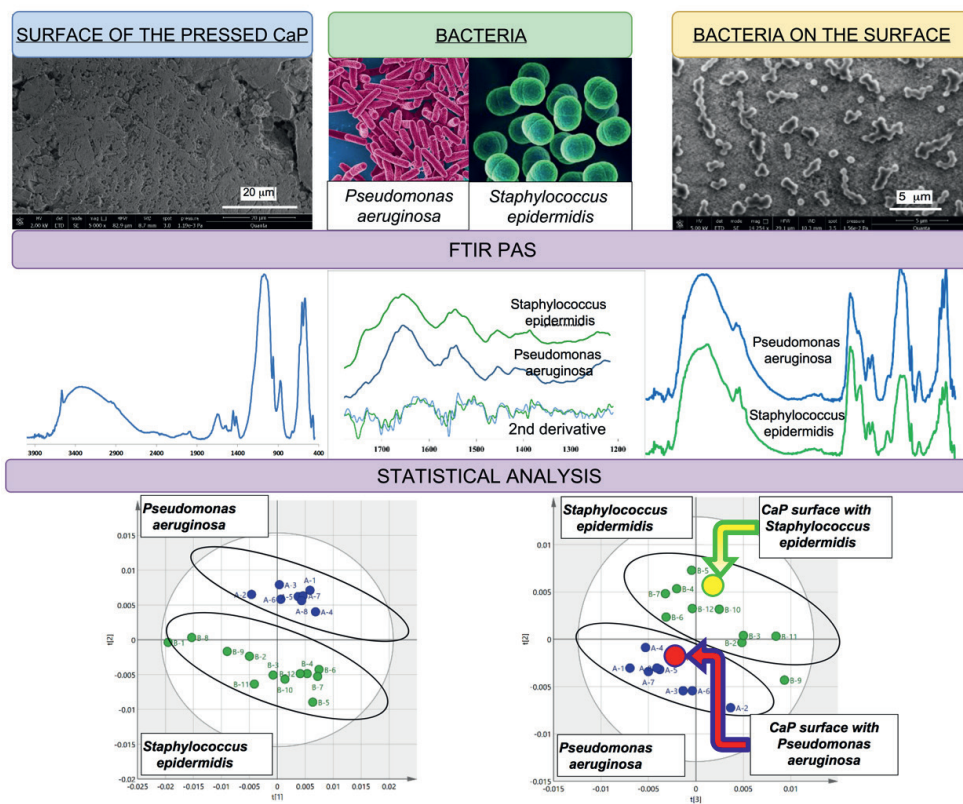


Fig. 30. The identification and recognition of bacteria using FTIR PAS and FTIR DRIFT methods.

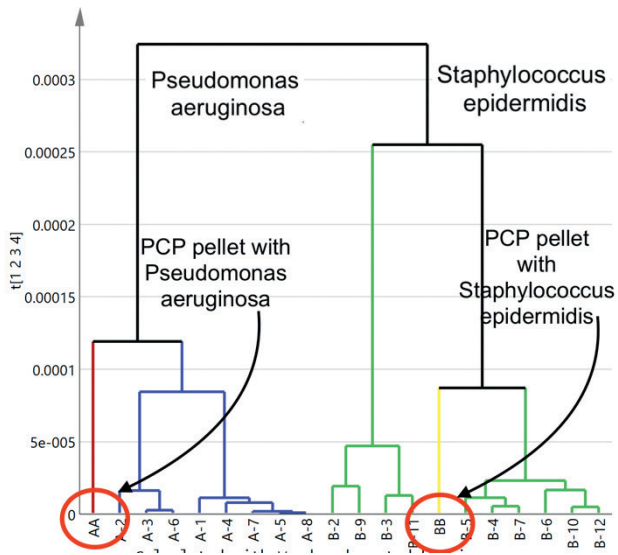


Fig. 31. The cluster analysis of *Pseudomonas aeruginosa* and *Staphylococcus epidermidis*.

### Conclusions

- a) FTIR PAS can be successfully used to study both calcium phosphate and bacteria on its surface at the same time.
- b) By supplementing the developed measurement method with statistical methods, it is possible to identify the type of bacteria directly on the surface of calcium phosphate (implant), which saves time spent on the colonization of bacteria and identification according to the standard method.

## CONCLUSION

1. In the study of nanosized calcium phosphates, FTIR PAS and DRIFT sampling techniques are the most appropriate methods for controlling the production process of amorphous or nanocrystalline calcium phosphate, which is difficult or impossible to implement with conventional FTIR sampling techniques:
  - for characterization of wet samples;
  - for the study of processes in volume (for instance, kinetics of the drying processes);
  - for the study of processes directly on the surface;
  - for automated data processing and analysis of samples *in-line* or *on-line* mode of the control system.
2. The developed model for the use of FTIR methods and multidimensional statistical analysis provides an opportunity to predict the particle size, degree of crystallinity, phase composition and carbonate composition (A, B type  $\text{CO}_3^{2-}$ ) of an unknown nanosized calcium phosphate sample. Analyzing of large amounts of data, makes it possible to carry out the automation of data processing and visualization, thus eliminating the subjectivity of data processing.
3. The developed model for FTIR methods and the deconvolution and convolution of spectra can be used:
  - for the simultaneous study of the surface of calcium phosphate (for instance, bioimplant) and bacteria, identification and differentiation;
  - in archeology, as an effective expression method for the identification of organic substances prior to the heavily expensive C-14 isotope analysis.
4. By combining FTIR methods with DTG method, it is possible to determine whether a product with a predicted moisture content (physically and chemically bound water) has been produced in the production process, which in turn allows predicting the stability of the product under storage conditions.

## REFERENCES

1. **Jochem, R.** *Was kostet Qualität? Wirtschaftlichkeit von Qualität ermitteln.* München: Carl Hanser Verlag, 2010, 1–25.
2. U. S. Department of Health and Human Services, Food and Drug Administration, Guidance for Industry, *PAT – a Framework for Innovative Pharmaceutical Development, Manufacturing and Quality Assurance*, FDA, Silver Spring, 2004, [online] – [retrieved 05/05/2017]. Available at: <http://www.fda.gov/cvm/guidance/published.html>
3. **Kessler, R.W.**, *Prozessanalytik. Strategien und Fallbeispiele aus der industriellen Praxis*, Weinheim: Wiley–VCH, 2006, 25–35.
4. **Kandelbauer, A., Rahe, M., Kessler, R. W.**, Industrial Perspectives. In: *Handbook of Biophotonics*, 2013, [online] – [retrieved 05/05/2017] Available at: <http://onlinelibrary.wiley.com/doi/10.1002/9783527643981.bphot082/abstract>
5. **Becker, T. and Krause, D.** Softsensorysysteme-Mathematik als Bindeglied zum Prozessgeschehen. *Chem. Ing. Tech.*, 2010, Vol. 82, No. 4, p. 429–440.
6. **Eichert D., Drouet C., Sfihi H.**, et.al. Nanocrystalline apatite-based biomaterials : Synthesis, processing and characterization. *Biomaterials research advances*, 2007, 93–143.
7. **Rey C., Combes C., Drouet C.**, et.al. Bioactive Ceramics: Physical Chemistry. In: P. Ducheyne, K.E. Healy, D.W. Hutmacher, D.W. Grainger, C.J. Kirkpatrick (eds.) *Comprehensive Biomaterials*, Elsevier, Amsterdam et. al., 2011, Vol. 1, p. 187–221.
8. **Smith B.C.** *Fundamentals of Fourier Transform Infrared Spectroscopy*, CRC Press, 2011, p. 20–65.
9. **Stuart B.H.** Infrared spectroscopy: Fundamentals and Applications. In: *Analytical Techniques in the Sciences*, 2005 [online] – [retrieved 05/05/2017]. Available at: <http://onlinelibrary.wiley.com/book/10.1002/0470011149>
10. **Bell A. G.** On the production and reproduction of sound by light, *Am. J. Sci.* 1880, Vol. S3–20, p. 305–324.
11. **Kauppinen J., Wilcken K., Kauppinen I.**, et.al. High sensitivity in gas analysis with photoacoustic detection. *Microchem. J.*, 2004, Vol. 76, p. 151–159.
12. **Roveri N., Iafisco M.** Evolving application of biomimetic nanostructured hydroxyapatite. *Nanotechnology, Science and Applications*, 2010, Vol.3, p. 107–125.
13. **Hench L.L., Polak J.M.** Third-generation biomedical materials. *Science*, 2002, Vol. 295, p. 1014–1017.
14. **LeGeros R.Z.** Calcium phosphate-based osteoinductive materials. *Chem Rev.*, 2008, Vol.108, No. 11, p. 4742–4753.
15. **Rey C., Lian J., Grynpas M.**, et.al. Non-apatitic environments in bone mineral: FT-IR detection, biological properties and changes in several disease states, *Connective Tissue Research*, 1989, Vol. 21, No. 1–4, p. 267–273.
16. **Combes C., Rey C.** Amorphous calcium phosphates: Synthesis, properties and uses in biomaterials. *Acta Biomater.*, 2010, Vol. 6, p. 3362–78.
17. **Elliott J.C., Wilson R.M., Dowker S.E.P.** Apatite Structures. *Adv. X-Ray Anal.*, 2002, Vol. 45, p. 172–181.
18. **Soenju Clasen A. B., Ruyter I. E.** Quantitative Determination of Type A and Type B Carbonate in Human Deciduous and Permanent Enamel By Means of Fourier Transform Infrared Spectrometry, *Adv. Dent. Res.*, 1997, p. 523–527.
19. **Lafon J. P., Champion E., Bernache-Assollant D.** Processing of AB-type carbonated hydroxyapatite  $\text{Ca}_{10-x}(\text{PO}_4)_6-x(\text{CO}_3)_x(\text{OH})_{2-x-2y}(\text{CO}_3)_y$  ceramics with controlled composition. *J. Eur. Ceram. Soc.*, 2008, Vol. 28, No. 1, p. 139–147.
20. **Markovic M., Fowler B.O., Tung M.S.** Preparation and comprehensive characterization of a calcium hydroxyapatite reference material, *J. Res. Natl. Inst. Stand. Technol.*, 2004, Vol. 109, p. 553–568.
21. **Mendelsohn R.** Fourier Transform Infrared Spectrometry. *J. Am. Chem. Soc.*, 2007, Vol. 129, No. 43, p. 13358, Oct.

22. **Gautam R., Vanga S., Ariese F.** Review of multidimensional data processing approaches for Raman and infrared spectroscopy. *EPJ Tech. Instrum.*, 2015, Vol. 2, No. 1, p. 8.
23. **Geladi P.** Chemometrics in spectroscopy. Part 1. Classical chemometrics. *Spectrochim. Acta B.*, 2003, Vol. 58, p. 767–82.
24. **Davis R., Mauer L.** Fourier transform infrared (FT-IR) spectroscopy: a rapid tool for detection and analysis of foodborne pathogenic bacteria. *Curr. Res. Technol. Educ. Top.* 2010, No. 1, p. 1582–1594.
25. **Maetschke S.R., Madhamshettiwar P.B., Davis M.J., et.al.** Supervised, semi-supervised and unsupervised inference of gene regulatory networks. *Briefings in Bioinformatics*, 2014, Vol. 15, No. 2, p. 195–211.
26. **Pollard, A.M., Heron, C.** *Archaeological Chemistry*. Cambridge: The Royal Society of Chemistry, 2008, 438 p.
27. **Naumann D., Labischinski H., Giesbrecht P.** The characterization of microorganisms by Fourier Transform Infrared Spectroscopy (FT/IR), *In: Modern Techniques for Rapid Microbiological Analysis* (Eds.), W. H. Nelson, VCH, New York, 1991, p. 43–96.

## APPENDIX

The schemes for the selection of the FTIR methods, spectrum processing and analysis show the main steps from taking a FTIR spectrum to making the conclusions.

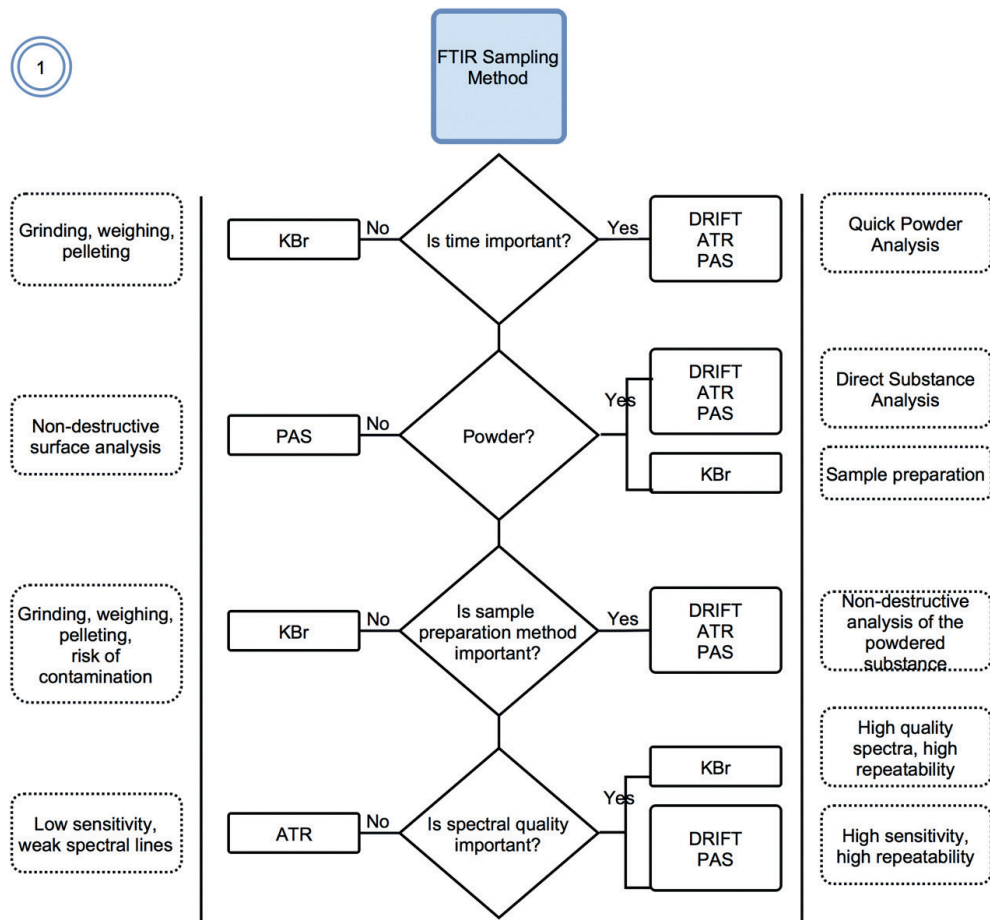


Fig. 1. The selection of the FTIR method for the study of nanosized calcium phosphate.

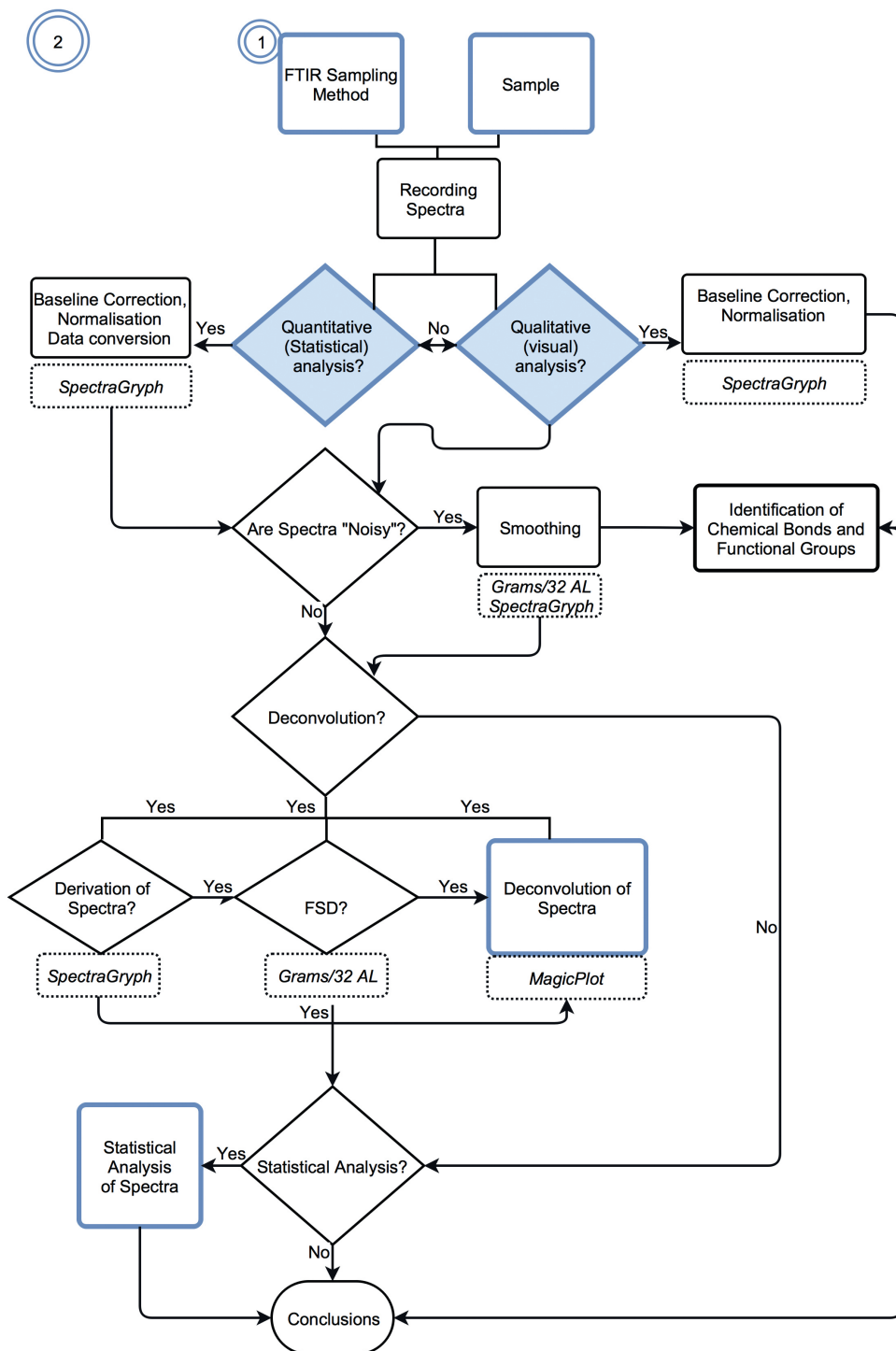


Fig. 2. The preparation of spectra for qualitative and quantitative analysis.

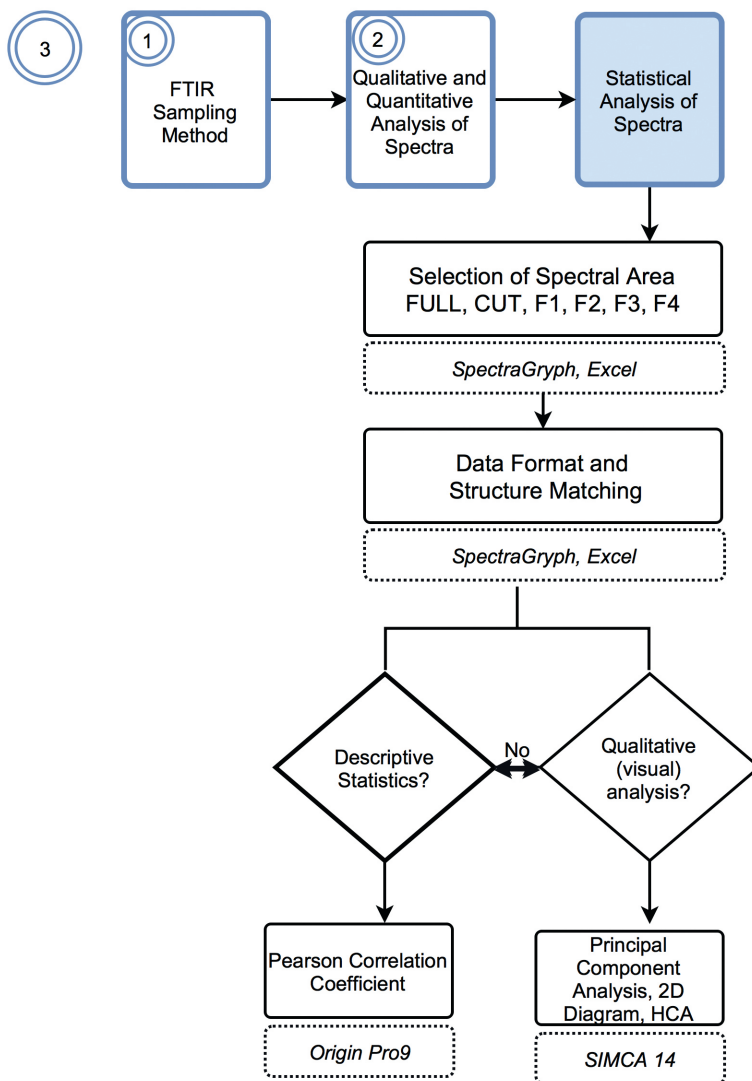


Fig. 3. The statistical analysis of spectra.